EPRI | ELECTRIC POWER RESEARCH INSTITUTE

Assessment and Mapping of the Riverine Hydrokinetic Resource in the Continental United States

2012 TECHNICAL REPORT

Assessment and Mapping of the Riverine Hydrokinetic Energy Resource in the Continental United States

EPRI | ELECTRIC POWER
RESEARCH INSTITUTE

1026880
Final Report, December 2012

DISCLAIMER OF WARRANTIES AND LIMITATION OF LIABILITIES

THE FOLLOWING ORGANIZATIONS, UNDER CONTRACT TO EPRI, PREPARED THIS REPORT:

University of Alaska Anchorage
University of Alaska Fairbanks
National Renewable Energy Laboratory

NOTE

For further information about EPRI, call the EPRI Customer Assistance Center at 800.313.3774 or e-mail askepri@epri.com.

Acknowledgments

Product Description

This report describes the methodology and results of the most rigorous assessment to date of the riverine hydrokinetic energy resource in the contiguous 48 states and Alaska, excluding tidal waters. The assessment provides estimates of the gross, naturally available resource, termed the theoretical resource, as well as estimates, termed the technically recoverable resource, that account for selected technological factors affecting capture and conversion of the theoretical resource. The technically recoverable resource does not account for all technical constraints on energy capture and conversion.

Background

The U.S. Department of Energy (DOE) funded the Electric Power Research Institute and its collaborative partners, University of Alaska – Anchorage, University of Alaska – Fairbanks, and the National Renewable Energy Laboratory, to provide an assessment of the riverine hydrokinetic resource in the continental United States.

Objectives

The goal of this project was to estimate the riverine hydrokinetic resource in the continental United States.

Approach

The project team derived an assessment of the hydrokinetic resource in the 48 contiguous states from spatially explicit data contained in NHDPlus, a geographic information system (GIS)-based database containing river segment-specific information on discharge characteristics and channel slope. The team estimated the segment-specific theoretical resource from these data using the standard hydrological engineering equation that relates theoretical hydraulic power (P_{th}, Watts) to discharge (Q, m^3 s^{-1}) and hydraulic head or change in elevation (ΔH, m) over the length of the segment, where γ is the specific weight of water (9800 N m^{-3}):

$$P_{th} = \gamma \, Q \, \Delta H$$

For Alaska, which is not encompassed by NHDPlus, the team manually obtained hydraulic head and discharge data from Idaho National Laboratory's Virtual Hydropower Prospector, Google Earth, and U.S. Geological Survey gages. The team estimated the technically recoverable resource by applying a recovery factor to the segment-specific theoretical resource estimates. This analysis, which included 32 scenarios, led to an empirical function relating recovery factor to slope and discharge. For Alaska, where data on river slope was not readily available, the recovery factor was estimated based on the flow rate alone.

Results

Segment-specific theoretical resource, aggregated by major hydrologic region in the contiguous, lower 48 states, totaled 1,146 TWh/yr. The aggregate estimate of the Alaska theoretical resource is 235 TWh/yr, yielding a total theoretical resource estimate of 1,381 TWh/yr for the continental United States. The technically recoverable resource estimate for the continental United States is 120 TWh/yr.

Results of this study can be geo-spatially visualized, queried, and downloaded from the National Renewable Energy Laboratory's website at: http://maps.nrel.gov/river_atlas. Currently, results are only available for the 48 contiguous states. Alaska will be added in the future.

Applications, Values, and Use

While the calculation of the technically recoverable hydrokinetic resource takes into account some important constraints, a fuller accounting of additional practical constraints on turbine deployment would further reduce the portion of the theoretical resource that is estimated to be recoverable. The practically recoverable resource remains an unknown – and perhaps small -- portion of the technically recoverable resource. Additional data, assumptions, and highly detailed analysis are required to reliably estimate the practically recoverable hydrokinetic resource.

Keywords

Hydrokinetic resources
Hydropower
Renewable resources

Executive Summary

The U.S. Department of Energy (DOE) funded the Electric Power Research Institute and its collaborative partners, University of Alaska – Anchorage, University of Alaska – Fairbanks, and the National Renewable Energy Laboratory, to provide an assessment of the riverine hydrokinetic resource in the continental United States. The assessment benefited from input obtained during two workshops attended by individuals with relevant expertise and from a National Research Council panel commissioned by DOE to provide guidance to this and other concurrent, DOE-funded assessments of water-based renewable energy. These sources of expertise provided valuable advice regarding data sources and assessment methodology.

The assessment of the hydrokinetic resource in the 48 contiguous states is derived from spatially-explicit data contained in NHDPlus – a GIS-based database containing river segment-specific information on discharge characteristics and channel slope. 71,398 river segments with mean annual flow greater than 1,000 cubic feet per second (cfs) mean discharge were included in the assessment. Segments with discharge less than 1,000 cfs were dropped from the assessment, as were river segments with hydroelectric dams. The results for the theoretical and technical resource in the 48 contiguous states were found to be relatively insensitive to the cutoff chosen. Raising the cutoff to 1,500 cfs had no effect on estimate of the technically recoverable resource, and the theoretical resource was reduced by 5.3%.

The segment-specific theoretical resource was estimated from these data using the standard hydrological engineering equation that relates theoretical hydraulic power (P_{th}, Watts) to discharge (Q, m^3 s^{-1}) and hydraulic head or change in elevation (ΔH, m) over the length of the segment, where γ is the specific weight of water (9800 N m^{-3}):

$$P_{th} = \gamma \, Q \, \Delta H$$

For Alaska, which is not encompassed by NPDPlus, hydraulic head and discharge data were manually obtained from Idaho National Laboratory's Virtual Hydropower Prospector, Google Earth, and U.S. Geological Survey gages. Data were manually obtained for the eleven largest rivers with average flow rates greater than 10,000 cfs and the resulting estimate of the theoretical resource was expanded to

include rivers with discharge between 1,000 cfs and 10,000 cfs based upon the contribution of rivers in the latter flow class to the total estimate in the contiguous 48 states.

Segment-specific theoretical resource was aggregated by major hydrologic region in the contiguous, lower 48 states (Table ES-1) and totaled 1,146 TWh/yr. The aggregate estimate of the Alaska theoretical resource is 235 TWh/yr, yielding a total theoretical resource estimate of 1,381 TWh/yr for the continental US.

The technically recoverable resource in the contiguous 48 states was estimated by applying a recovery factor to the segment-specific theoretical resource estimates. The recovery factor scales the theoretical resource for a given segment to take into account assumptions such as minimum required water velocity and depth during low flow conditions, maximum device packing density, device efficiency, and flow statistics (e.g., the 5 percentile flow relative to the average flow rate). The recovery factor also takes account of "back effects" – feedback effects of turbine presence on hydraulic head and velocity. The recovery factor was determined over a range of flow rates and slopes using the hydraulic model, HEC-RAS. In the hydraulic modeling, presence of turbines was accounted for by adjusting the Manning coefficient. This analysis, which included 32 scenarios, led to an empirical function relating recovery factor to slope and discharge. Sixty-nine percent of NHDPlus segments included in the theoretical resource estimate for the contiguous 48 states had an estimated recovery factor of zero. For Alaska, data on river slope was not readily available; hence, the recovery factor was estimated based on the flow rate alone. Segment-specific estimates of the theoretical resource were multiplied by the corresponding recovery factor to estimate the technically recoverable resource. The resulting technically recoverable resource estimate for the continental United States is 120 TWh/yr (Table 1).

Table 1
Theoretical and technically recoverable hydrokinetic energy estimates for the continental United States.

Hydrologic Region	Theoretical Power (Annual Energy ,TWh/yr)	Technically Recoverable Power (Annual Energy, TWh/yr)
New England	14.4	0.2
Mid Atlantic	33.5	1.0
South Atlantic Gulf	38.5	1.2
Great Lakes	6.2	0.01
Ohio	79.2	6.9
Tennessee	20.4	1.0
Sauris Red-Rainy	1.8	0.03
Upper Mississippi	47.0	5.1
Lower Mississippi	208.8	57.4
Texas Gulf	8.9	0.05
Arkansas Red	45.1	1.3
Lower Missouri	79.8	5.6
Upper Missouri	74.3	2.8
Rio Grande	29.5	0.3
Lower Colorado	57.6	3.9
Upper Colorado	46.9	1.1
Great Basin	6.9	0
California	50.9	0.7
Pacific Northwest	296.7	11.0
Alaska	235	20.5
Total	**1,381**	**119.9**

The Lower Mississippi region contributes nearly half (47.9%) of the total resource estimate. The major rivers of Alaska constitute 17.1% of the total for the continental U.S. The next largest contributor is the Pacific Northwest region, which contributes 9.2%, followed by the Ohio region (5.7%). Collectively these four regions encompass 80% of the technically recoverable hydrokinetic resource in the continental U.S.

While the calculation of the technically recoverable hydrokinetic resource takes into account some important constraints, a fuller accounting of additional practical constraints on turbine deployment would further reduce the portion of the theoretical resource that is estimated to be recoverable. The practically recoverable resource remains an unknown – and perhaps small -- portion of the technically recoverable resource. Additional data, assumptions, and highly detailed analysis are required to reliably estimate the practically recoverable hydrokinetic resource.

Results of this study can be geo-spatially visualized, queried, and downloaded from the National Renewable Energy Laboratory's website at: http://maps.nrel.gov/river_atlas. Currently, results are only available for the 48 contiguous states. Alaska will be added in the future.

Table of Contents

List of Figures

List of Tables

Section 1: Introduction and Background

This report describes the methodology and results of the most rigorous assessment to date of the riverine hydrokinetic energy resource in the contiguous 48 states and Alaska, excluding tidal waters. The assessment provides estimates of the gross, naturally available resource, termed the theoretical resource, as well as estimates, termed the technically recoverable resource, that account for selected technological factors affecting capture and conversion of the theoretical resource. The technically recoverable resource, as defined in this study does not account for all technical constraints on energy capture and conversion.

The practical resource – the resource that could be recovered considering additional factors such as existing uses, environmentally sensitive and other exclusion areas, economic constraints, and access to load or transmission – is an unknown fraction of the technically recoverable resource. This report does not provide an assessment of the practical resource; nor does it provide the information needed to site projects. Far more detailed study is required to estimate the practical resource and to select candidate sites for hydrokinetic project development.

This report is intended to provide policymakers, project developers, hydrokinetic energy device developers, investors, universities, non-governmental organizations, environmental groups, the U.S. Department of Energy (DOE), the military, and the U.S. Army Corps of Engineers and the U.S. Geological Survey an assessment of the general magnitude and geographic distribution of the riverine hydrokinetic resource across the continental United States.

The DOE previously commissioned a study of the U.S. hydrokinetic energy resource (Miller *et al.* 1986). That study derived estimates of hydrokinetic power for selected river segments in 12 of 16 hydrologic regions of the U.S. with mean discharge of at least 4,000 cubic feet per second (cfs) and velocity greater than 4.3 feet per second (fps). Within each of the regions in which these criteria were met, the rivers with the greatest potential were selected for assessment. This procedure provided estimates of recoverable power in the rivers with the greatest potential in each of the regions meeting the minimum criteria; however, the criteria for inclusion in the study differed among regions. Recoverable power was estimated assuming turbine deployment in 25% of the estimated width and 25% of river segment lengths meeting the minimum discharge criteria, turbine diameter equal to 80% of the mean depth, turbine spacing of half a turbine diameter space between turbines in each row and 5 turbine diameters spacing between rows, and system efficiency of 40%. Miller *et al.* (1986) did not include

the feedback effects of turbine deployment on water velocity. The foregoing methodology applied to the selected river segments yielded an aggregate power estimate slightly greater than 12,500 MW average annual power (110 TWh/yr). There are no other broad-scale riverine hydrokinetic resource assessments for the United States. Canada is currently conducting an assessment of its riverine hydrokinetic resource (NRC-CHC 2010).

The present assessment improves upon the estimate of Miller *et al.* (1986) in a number of ways. It includes the potential energy associated with hydraulic head as well as the back effects of turbine deployment. It also applies a consistent criterion for inclusion across the contiguous 48 states, and explicitly assesses a larger number of rivers in Alaska. The threshold for inclusion in this assessment is 1,000 cfs mean discharge, making the present assessment more comprehensive in its scope. This assessment, however, makes different assumptions regarding turbine deployment, leading to a flow threshold for hydrokinetic energy recovery of 7,000 cfs mean discharge.

The choice of databases selected for this study, as well as the underlying methodology and analytical assumptions, benefited from advice acquired in two expert workshops. The project also benefited from review and input by a committee of the National Research Council that was commissioned by DOE to review this resource assessment and the related, DOE-funded assessments of other water-based resource types.

Definition of the Theoretical and Technical In-Stream Hydrokinetic Resource

The in-stream (non-tidal) hydrokinetic power *theoretically* available in a given river segment (P_{th}, Watts) is defined:

$$P_{th} = \gamma\, Q\, \Delta H \qquad\qquad\qquad \textit{Eq. 1-1}$$

where γ is the specific weight of water (~9800 N m^{-3}),

      Q is the flow rate (m^3/s), and

      ΔH (m) is the change in hydraulic head between the beginning and end of the river segment.

The in-stream hydrokinetic power *technically* recoverable in a given river segment (P_{tech}, Watts) is the portion of the theoretically available power that can be recovered given selected technical constraints and assumptions, including:

a)   water depth at the 5-percentile flow (the flow exceeded 95% of the time) greater than or equal to 2.0 m,

b)   depth-averaged velocity of the 5-percentile flow greater than or equal to 0.5 m/s,

c) "rule-of-thumb" device spacing, and

d) 30% "water to wire" device efficiency including efficiencies of: rotor, gearbox, generator, frequency converter, and step-up transformer (EPRI 2008).

The technically available hydrokinetic power estimates incorporate "back effects" – feedback effects of energy extraction on river depth and velocity. Section 4 provides a detailed description of the methodology used to estimate the technically recoverable resource.

Section 2: Methodology for Estimating the Theoretically Available In-stream Hydrokinetic Resource

This section describes the methodology for estimating the theoretically available, non-tidal, riverine hydrokinetic resource. Consultation with an expert panel convened in April 2010 to support this assessment identified NHDPlus as the most suitable hydrography dataset for assessment of the hydrokinetic resource. Currently, the NHDPlus database covers the 48 contiguous states, but does not encompass Alaska; consequently, a different data source and methodology are required for the State of Alaska. NHDPlus is described briefly below. Additional information and documentation is available at: www.horizon-systems.com/nhdplus/.

Contiguous 48 States

Mapping data exists to estimate the available power from the rivers in the contiguous United States. This mapping data is in the form of a geographic information system (GIS) and is part of the US National Map developed by the US Geological Survey (USGS). The GIS layer of the US National Map with river data is the National Hydrography Dataset (NHD). In addition to rivers, NHD includes other hydrographic features such as shorelines, lakes and ponds, as well as canals and aqueducts.

The Environmental Protection Agency (EPA) collaborated with the USGS to enhance NHD to support EPA's water quality modeling activities. The enhanced GIS database, called NHDPlus, represents hydrologic networks as networks of "flowlines". Individual flowlines range in length from 1m to 41km, and each has an assigned average velocity, discharge, and slope. These flowlines and associated data constitute the basic geo-spatial units of analysis for the portion of this study encompassing the 48 contiguous states. We use the term segments to refer to these geo-spatial units of analysis.

Figure 2.1 below shows NHDPlus flowlines for the Mississippi, Missouri, and Illinois rivers at St Louis, Missouri overlaid on a map of the area. The arrowhead at the bottom of each flowline indicates the direction of flow. This example illustrates discrepancies between the flowlines in NHDPlus and river courses depicted in a more recent map.
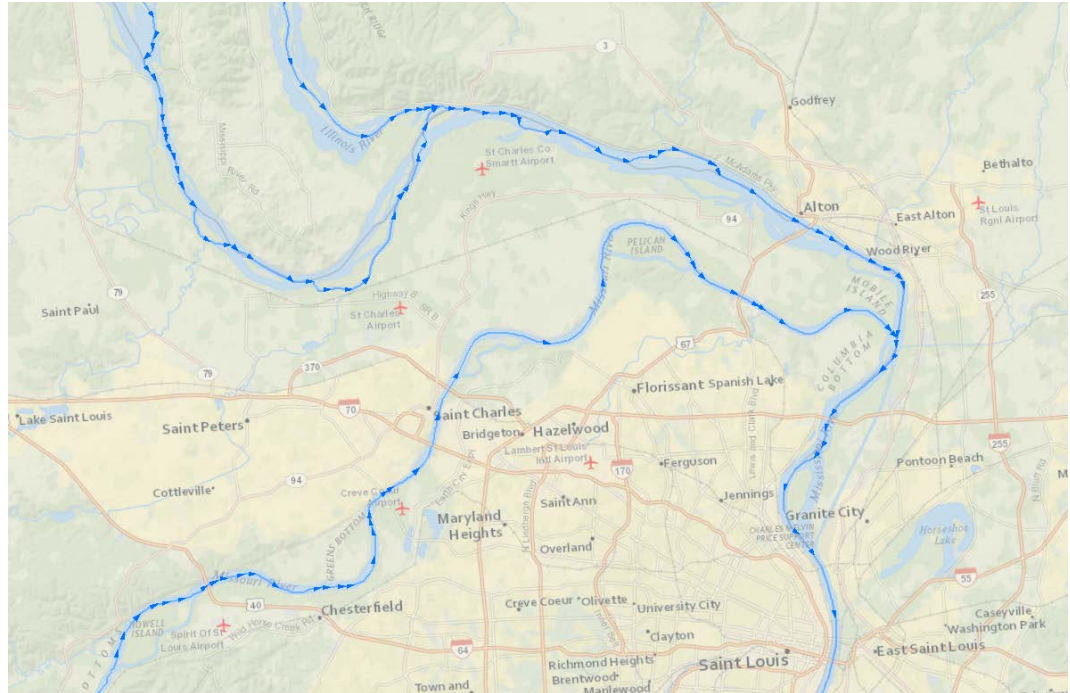
Figure 2-1
Flowlines of various lengths and downstream directions near St Louis.

Theoretical power is estimated according to Equation 1.1, using the segment–specific average water discharge (Q) provided by NHDPlus in units of cubic feet per second (cfs). Hydraulic head (ΔH) is calculated from segment length and slope. Figure 2.2 shows GIS data for a number of NHDPlus flowlines (segments). NHDPlus provides two estimates of annual discharge but only one (MAFLOWU) is available in all of the river segments. Hence, the " MAFLOWU" estimate of discharge is used in this study.

FID	GNIS_ID	GNIS_NAME	LENGTHKM	MAFLOWU	SLOPE
28099	00410769	Illinois River	3.123	19354.46285	0.00005
28098	00410769	Illinois River	2.349	19381.40913	0.00005
28101	00410769	Illinois River	1.169	19383.53753	0.00005
28103	00410769	Illinois River	0.743	19385.28085	0.00005
28105	00410769	Illinois River	0.549	19387.38693	0.00053
28096	00410769	Illinois River	0.488	19387.42247	0.00005
42990	00485180	Missouri River	6.224	75076.37628	0.00019
42982	00485180	Missouri River	8.39	75083.98222	0.00018
42980	00485180	Missouri River	1.384	75085.35546	0.00005
42981	00485180	Missouri River	0.792	75087.00404	0.00005
42983	00485180	Missouri River	0.998	75088.94296	0.00005
42984	00485180	Missouri River	2.415	75090.7423	0.0001
42985	00485180	Missouri River	1.668	75092.91206	0.00005
27301	00465962	Mississippi River	1.453	77804.99981	0.00005
27302	00465962	Mississippi River	1.44	77929.90734	0.00001
27313	00465962	Mississippi River	4.884	77937.43923	0.00009
27282	00465962	Mississippi River	1.511	77937.65775	0.00013
27279	00465962	Mississippi River	0.604	77938.16869	0.00005
27278	00465962	Mississippi River	2.249	77940.91354	0.00005
27273	00465962	Mississippi River	0.985	77948.44491	0.00005
27304	00465962	Mississippi River	1.362	77948.68373	0.00065

(44 out of 72408 Selected)

velocity unfiltered

Figure 2-2
Screenshot of NHDPlus data showing flowline identifier (FID), Geographic Names Information System ID (GNIS_ID), river name (GNIS_NAME), length (LENGTHKM, km), computed mean annual flow (MAFLOWU, cfs), and average slope (SLOPE, unitless rise over run).

Preparing the Data

This assessment is limited to the riverine hydrokinetic resource; thus, NHDPlus records pertaining to lakes, reservoirs, ponds, etc. are excluded from the analysis. Smaller rivers and stream segments with discharge of less than 1,000 cubic feet per second (cfs) are also excluded. The minimum flow criterion was selected in consultation with the expert panel convened on April 27, 2011.

Segments containing dams with hydroelectric plants were also excluded from analysis. Existing hydroelectric generating facilities for the analysis were determined using licensed data from the Homeland Security Infrastructure Program (HSIP). Hydroelectric plants were spatially referenced by feature intersection with the NHDPlus data using a 0.25 mile buffer around the HSIP hydroelectric plants. River segments that were intersected within the buffer were analyzed by their delta-H attribute (difference in elevation between segment endpoints) and ranked in order from largest to smallest. The river segments with the largest delta-H values from each hydroelectric plant buffer area were selected as the segment most likely to contain the dam. A limited number of

hydroelectric dams were not included in the results of initial spatial analysis, most often due to distances greater than 0.25 miles between the power house and the original river channel that was used to map the river in-stream data. These occurrences were handled by comparing the HSIP Electric Power Plant locations with the publically available National Inventory of Dams (NID) data locations. Where applicable, the search bounds were increased to intersect these locations with the river in-stream data. The same methodology from the initial analysis was applied to the intersected river segments within the increased search area for selecting the river segment with the greatest delta-H attribute. These segments were appended to the results from the initial spatial analysis, and all segments identified in this manner were excluded from the resource assessment.

These exclusionary criteria reduced the number of NHDPlus records from 2.9 million to 71,398 records.   Figure 2.3 shows the rivers with mean discharge greater than 1,000 cfs in the contiguous United States which are included in the assessment, and the hydrologic basins by which results are aggregated for presentation. Note that several of the basins extend north into Canada and south into Mexico; however those areas were excluded from the analysis.

Figure 2-3
Riverine resources and hydrographic regions for which the theoretical power is calculated.

Alaska

Since NHDPlus does not encompass Alaska, alternative sources were used to obtain input values for the theoretical power equation ($\gamma Q \Delta H$). Average discharge data was obtained from USGS gages to the extent possible. Where USGS gage data was lacking, we obtained average discharge data from the Virtual Hydropower Prospector (the Prospector) developed for Alaska by the Idaho National Laboratory (http://hydropower.inel.gov/prospector/index.shtml). The discharge data from the Prospector and USGS gages at selected sites was generally similar. Table 2.1 compares discharge data from the Prospector and from USGS gages at four examples sites. On average, the Prospector's estimate of annual average discharge was 25% higher than that based on USGS measurements. By far, the deviation between the Prospector discharge estimate and the USGS measurement was greatest at Eagle on the Yukon River. Ignoring this outlier, the Prospector estimate was within 10% of the USGS measurement. USGS discharge measurements were used for the estimate of the theoretical resource in the Yukon River.

Table 2-1
Analysis of discharge data from the Prospector and from USGS gages for the Alaska portion of the study.

Location	River	Prospector	USGS	Difference
		(cfs)	(cfs)	%
Eagle	Yukon	148100	84000	76.3
Crooked Creek	Kuskokwim	54300	42000	29.3
Hughes	Koyukuk	14800	14600	1.4
Million Dollar Bridge	Copper	61300	61900	-1.0
			Average:	26.5 %

Hydraulic head change in the river segments was estimated based on river surface elevations from the Prospector or from Google Earth. A comparison of surface elevations from the Prospector and Google Earth indicated they yield similar results (Table 2.2). The discharge at the segment ends (which differed significantly in some instances) was averaged to obtain the segment discharge for the theoretical power calculation.

Table 2-2
Analysis of elevation change data from Google Earth and from the Prospector for the Alaska portion of the study.

Segment Start	Segment End	Elevation Difference from Google Earth (m)	Elevation Difference from the Prospector (m)	Percent Difference
Eagle, Yukon River	Stevens Village, Yukon River	224.4	221.1	1
Crooked Creek, Kuskokwim River	Bethel, Kuskokwim River	41.2	40.4	2
Talkeetna, Susitna River	Mouth of Susitna River, Cook Inlet	99.7	107.0	-7

This methodology was first used to estimate the theoretical power for segments with mean discharge exceeding approximately 10,000 cfs in the following major rivers:

- Yukon
- Porcupine
- Kuskokwim
- Tanana
- Susitna
- Colville
- Stikine
- Kvichak
- Nushagak
- Noatak
- Copper

In order to estimate the theoretical resource in Alaska for flows between 1,000 cfs and 10,000 cfs, an analysis of the contribution to the theoretical resource from segments with discharge above and below 10,000 cfs was conducted for the 19 hydrologic regions in the NHDPlus database (which was available for the contiguous US). For each of the 19 regions in the NHDPlus database, the ratio of the theoretical power from flows above 10,000 cfs to power from flows above 1,000 ($R_{10,000/1,000}$) was determined. Further, that ratio was examined as a function of the maximum annual flow rate in the region (Figure 2.4). It was anticipated that regions with very large rivers (e.g., the Lower Mississippi) would have a relatively large fraction of its theoretical resource coming from segments with flow rate above 10,000 cfs. Hence, $R_{10,000/1,000}$ would be quite high approaching 1. The data in Figure 2.4 confirms this idea. Based on the logarithmic regression equation in the figure, and given a maximum annual discharge in Alaska of

272,000 cfs, $R_{10,000/1,000}$ for Alaska was estimated to be 0.75. Finally, the theoretical resource (for $Q > 1,000$ cfs) was estimated to be 1.33 times the theoretical resource for discharges greater than 10,000 cfs.

The chart shows a scatter plot with a logarithmic trend line. The y-axis is labeled $R_{10,000/1,000}$ and ranges from 0 to 1.2. The x-axis is labeled "flow rate (cfs)" and ranges from 0 to 800,000. The equation and correlation shown are:

$$y = 0.1884\ln(x) - 1.5713$$
$$R^2 = 0.5613$$
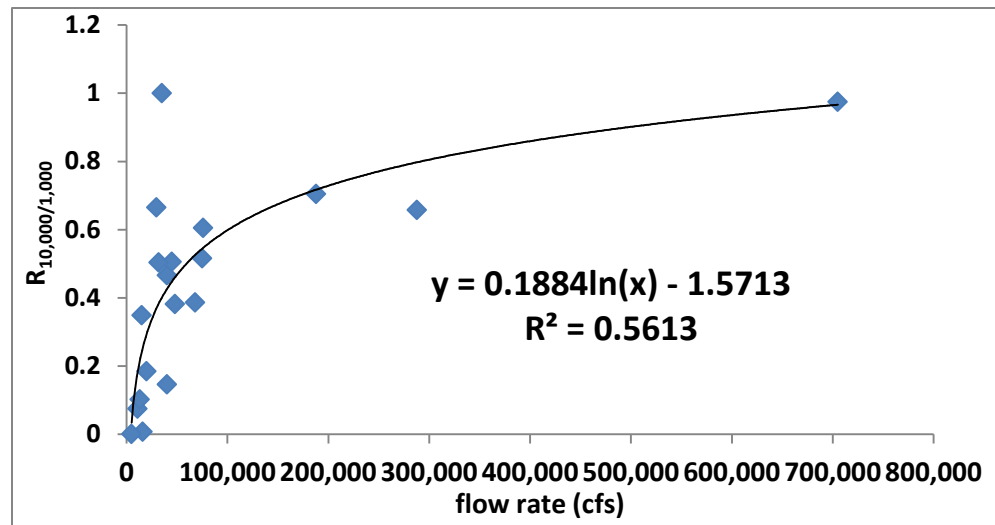
Figure 2-4
Ratio of the theoretical power from flows above 10,000 cfs to power from flows above 1,000 ($R_{10,000/1,000}$) for the 19 hydrologic regions of the contiguous US as a function of maximum annual discharge rate in that region.

An alternative estimate of $R_{10,000/1,000}$ for Alaska would be to ignore the dependence of the ratio on discharge and simply determine $R_{10,000/1,000}$ considering all of the regions of the contiguous US. In that case, the ratio would be 0.615 and the aggregate estimate for Alaska segments with discharge exceeding 10,000 cfs would be multiplied by 1.63 to obtain an estimate of statewide theoretical power in segments exceeding 1,000 cfs. Given the relatively high R^2 value in Figure 2.4, the former approach was adopted.

Section 3: Results for Theoretically Available Hydrokinetic Resource

The estimate of the theoretical resource for the continental United States (contiguous 48 states and Alaska) totals 1,381 TWh/yr (Table 3.1). Collectively, the Pacific Northwest, Lower Mississippi, and Alaska regions comprise 54% of the total estimated theoretical resource. Appendix C reports the theoretical resource estimates for the major rivers in Alaska. Expansion of the results detailed in Appendix C to account for the theoretical power in rivers of discharge between 10,000 and 1,000 cfs as described in Section 2 yields a total Alaska resource estimate of approximately 235 TWh/yr. The Yukon River had a theoretical resource of 80.5 TWh/yr and was the largest contributor to Alaska's hydrokinetic power potential.

Table 3-1
Theoretical power (annual energy) presented in units of terawatt hours per year aggregated by hydrologic regions that are depicted in Figure 3.1 and Alaska.

Hydrologic Region	Theoretical Power (Annual Energy ,TWh/yr)
New England	14.4
Mid Atlantic	33.5
South Atlantic Gulf	38.5
Great Lakes	6.2
Ohio	79.2
Tennessee	20.4
Sauris Red-Rainy	1.8
Upper Mississippi	47.0
Lower Mississippi	208.8
Texas Gulf	8.9
Arkansas Red	45.1
Lower Missouri	79.8

Table 3-1 (continued)
Theoretical power (annual energy) presented in units of terawatt hours per year aggregated by hydrologic regions that are depicted in Figure 3.1 and Alaska.

Hydrologic Region	Theoretical Power (Annual Energy ,TWh/yr)
Upper Missouri	74.3
Rio Grande	29.5
Lower Colorado	57.6
Upper Colorado	46.9
Great Basin	6.9
California	50.9
Pacific Northwest	296.7
Alaska	235
Total	**1,381**

Section 4: Methodology for Estimating the Technically Recoverable In-Stream Hydrokinetic Resource

The technically recoverable in-stream hydrokinetic resource can be broadly defined as the amount of power that could be recovered given existing technologies. The technically recoverable resource is operationally defined by the methodology for estimating the fraction of the theoretically available resource that is technically recoverable. We refer to the scalar applied to the theoretical resource as the "recovery factor". The recovery factor, which is a function of the river slope and average discharge, was evaluated and applied by river segment. The technically recoverable resource was determined by assigning a recovery factor to each river segment in the database and determining the product of the recovery factor and the theoretical resource, and summing across segments.

A number of studies and reviews address the recoverable hydrokinetic resource in tidal settings (e.g., Couch and Bryden 2004, Garrett and Cummins 2005, Bryden and Couch 2006, EPRI 2006, Garrett and Cummins 2007, Lunden and Bahaj 2007, Sutherland *et al.* 2007, Blanchfield *et al.* 2008, Garrett and Cummins 2008, Karsten *et al.* 2008, Polagye *et al.* 2008, Sun *et al.* 2008, Walkington and Burrows 2009, Atwater and Lawrence 2010, Shapiro 2010, Defne *et al.* 2011, Yang and Wang 2011); however, there is no known, definitive study published on the recoverable *river in-stream* hydrokinetic resource other than the 1986 study by Miller *et al.* Ortgega-Achury *et al.* (2010) specifically addressed riverine hydrokinetics as well as other hydrokinetic technologies, but focused on the hydraulic and environmental consequences of turbine deployment rather than on the amount of recoverable energy in rivers.

One of the first studies to address energy extraction in a tidal context (Garrett and Cummins 2005) examined a constricted channel connecting two large bodies of water in which the tides at both ends were assumed to be unaffected by the currents through the channel. The turbines were assumed to be a uniform "fence" deployed across the channel. By assuming the water level difference between channel entrance and exit to be *a cos wt* (where *w* is the angular frequency and *a* is the tidal amplitude), Garrett and Cummins determined a maximum average power available of approximately: $0.22 \gamma a Q_{max}$, where Q_{max} is the maximum volumetric discharge in the channel (with no devices present). Given the resemblance of the Garrett and Cummins expression to our equation for the

theoretical resource (Eq. 1.1), it would be tempting to assume that 22% of the riverine theoretical resource is recoverable. That is, 0.22 might be taken as a first estimate of the riverine recovery factor. The nature of tidal and riverine channels and their respective flows, however, are fundamentally different. For example, unsteady flow and flow acceleration are critically important characteristics of tidal flow. Furthermore, in their treatment of the tidal problem, Garrett and Cummins (2005) included flow separation as the flow exits the channel. Riverine channel flow, however, readily can be treated as steady, non-accelerating flow without flow separation issues. Tidal and riverine flows also differ very dramatically in the way they will respond to deployments of increasing numbers of hydrokinetic devices. Garrett and Cummins (2005) explain that in tidal channels, the discharge tends to decrease as the number of devices becomes excessively large. In contrast, discharge is independent of the number (or density) of devices deployed in a riverine channel. Finally, while Garrett and Cummins (2005) establish the theoretical resource for a tidal system under the conditions assumed, it does not address the technically recoverable energy by accounting for factors such as minimum flow depths and velocities and spatial constraints on turbine deployment.

This project determines the recovery factor for riverine channels based on fundamental river hydraulic principles, and incorporates realistic depth, velocity, and device spacing constraints developed in consultation with device and project developers.

The recovery factor methodology assumes a simplified geometry – a "V" shaped river cross-section – with a side-slope of 0.06 based on the measured cross-river geometries of 21 river cross-sections (4 from the Mississippi River, 5 from the Columbia River, 3 from the Snake River, 4 from the Connecticut River, 2 from the Savannah River, 2 from the Willamette River, and 1 from the Kuskokwim River). Assuming a V-shaped channel and a single side slope value is somewhat arbitrary; however, the sensitivity study described in Section 6 indicates that the recovery factor is relatively insensitive to side slope. The recovery factor methodology also assumes a cumulative distribution function for "normalized" discharge (discharge divided by the average discharge). The cumulative distribution function for normalized discharge was based on USGS statistics for the Mississippi River at Vicksburg, Mississippi (Table 4.1). Flow statistics from a lower Mississippi River gage were chosen since the lower Mississippi is the dominant source of US hydrokinetic energy. River bottom roughness is represented using a Manning roughness coefficient (n) of 0.03 s m$^{-1/3}$.

Table 4-1
Discharge statistics assumed for recovery factor calculations based on measured discharge statistics from Vicksburg on the Mississippi River. The normalized discharge is the discharge relative to the annual average (17,000 m³/s).

Discharge percentile	Normalized Discharge
5%	0.18
25%	0.34
50%	0.60
75%	1.18
95%	3.18

Recovery Factors were calculated for selected combinations of 7 river slopes (0.005, 0.002, 0.001, 0.0005, 0.0003, 0.0001, 0.00002) and 7 discharges (20000, 10000, 3000, 1000, 400, 200, and 100 m³/s, Table 4.2) in three steps. First, the power theoretically available over a 1000 m length of channel was determined using Eq. 1 from Section 2 ($P_{th} = \gamma\, Q\, \Delta H$). Next, the technically recoverable power was determined (following the procedure described below). Finally, the ratio of the technically recoverable to theoretically available power was determined. Note that not all 49 combinations of discharge and slope were evaluated. Some scenarios were skipped either because it was clear prior to evaluation that they were well outside of the envelope of conditions suitable for turbine deployment (i.e., too shallow) or because they constituted unrealistic or rare conditions (e.g., high slope in combination with high discharge).

The technically recoverable power was determined using a HEC-RAS flow model. The first step was to determine the portion of the channel cross-section in which flow velocity and depth would be sufficient for hydrokinetic device deployment. An expert panel, convened in Washington D.C., during April 2011 advised that velocity and depth should exceed 0.5 m/s and 2 m, respectively, during low (5th percentile) flow conditions. Using the idealized ("V" shaped) channel, the distribution of velocity and water depth for the 5-percentile flow (Q_5) was calculated using the HEC-RAS model. Figure 4.1 below shows an example calculation of the distribution of velocity and depth for Q_5 = 1,800 m³/s and river slope = 0.0001. The average flow rate was 10,000 m³/s. Areas of insufficient depth (h_5 < 2 m) *or* insufficient velocity (V_5 < 0.5 m/s) were designated in HEC-RAS as the "left bank" and "right bank". Here, h_5 and V_5 refer to the 5-percentile depth and depth-averaged velocity, respectively.
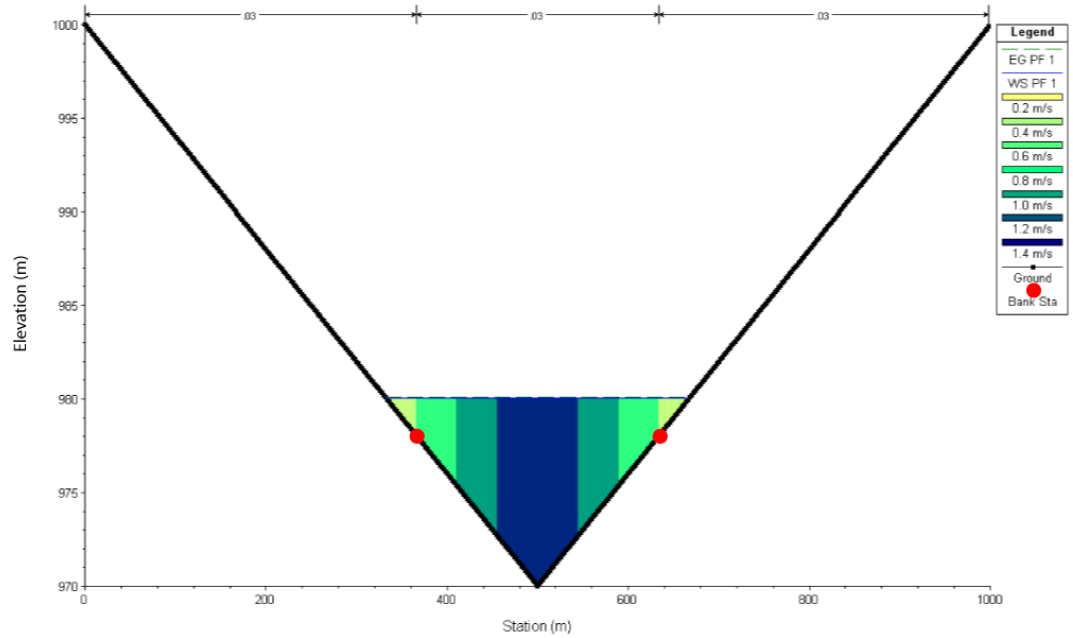
Figure 4-1
Display of calculated velocity and depth in idealized "V-shaped" channel for Q_5 =
1800 m^3/s and river slope = 0.0001. The red dots indicate the left and right bank
areas.

 Secondly, hydrokinetic devices were deployed (virtually) in the portion of the
river cross-section with sufficient depth and velocity (i.e., between the red dots in
Figure 4.1). Note, in this instance, deployment in the left and right bank areas is
restricted due to depth limitations. The devices were deployed according to "rule
of thumb" spacing. Specifically, it was assumed that devices would be deployed in
rows. Rows of devices were separated by a distance of 10 D where D is the device
diameter. Devices in a given row were separated by 2 D. The device diameter was
assumed to be 80% of the average depth in deployment area (at the 5 percentile
flow). The presence of the hydrokinetic devices would slow the flow of water in
the channel (i.e., cause "back effects"). To determine these back effects, the
presence of hydrokinetic devices was represented within HEC-RAS by
computing an effective bottom-roughness. The effective roughness (referred to
as n_t) was determined based on the roughness of the natural channel bottom (n),
the energy extraction of the hydrokinetic devices, and additional energy losses
associated with the mixing of the low velocity wake water with high velocity
water outside the wake. Based on a series of hydraulic calculations (Appendix B,
Kartezhnikova and Ravens in review), it was determined that:

$$n_t = n \cdot \left(b^{1/3} - 0.28263 \cdot b^{-1/3} + 0.139296\right)^{5/3} \qquad \text{\textit{Eq. 4-1}}$$

where:

$$b = 0.46088 \cdot a + ((0.46088 \cdot a + 0.68368)^2 + 0.022578)^{1/2} + 0.68368,$$

$$a = \left(\frac{3}{4} \frac{\xi\,(1+\epsilon)}{n^2 g} \cdot \frac{NA_r}{wL}\right) \cdot h^{1/3},$$

ξ is device efficiency,

ϵ is blockage ratio (fraction of river cross-section occupied by devices),

N is the number of devices in the river segment under consideration,

A_r (m^2) is the frontal (or swept) area of the device,

h (m) is water depth,

w (m) is the width of the river or channel that is occupied by devices, and

L (m) is the segment length.

Note, recent research (Ravens *et al.* in preparation) has shown that hydraulic impacts of hydrokinetic device deployments – as calculated using the enhanced roughness approach – are in agreement with hydraulic impacts as calculated using EFDC-based software developed by Sandia Labs (Jesse Roberts, Sandia National Laboratory; personal communication). Using the enhanced bottom roughness (n_t) to represent the devices, the average velocity (V, m/s) in the device deployment area was computed for the 5-, 25-, 50-, 75-, and 95-percentile flow rates (Table 4.1). In addition, the extracted power (i.e., technically available power) for each flow rate was calculated using:

$$P_{tech} = \xi \, \frac{\rho}{2} V^3 (NA_r) \qquad\qquad\qquad \textit{Eq. 4-2}$$

Finally, the ratio of the technically recoverable power to theoretically available power (i.e., the recovery factor) was calculated for each discharge. The recovery factor at a given river segment was observed to decrease with increasing discharge. For example, the recovery factor for the various discharges is provided for a channel with an average discharge of 10,000 and for a slope of 0.0005 (Table 4.2). The weighted average recovery factor is 0.24 which is approximated by the recovery factor for the 50-percentile discharge. Table 4.2 also reports the average flow depth in the deployment area with and without hydrokinetic devices deployed. The data shows that the impact of the devices on water level increases with flow rate. Finally, Table 4.2 shows how the blockage ratio – the ratio of the turbine swept area to the cross-sectional area - varies with flow rate (at a given location). Three calculations of blockage ratio are provided in Table 4.2.

Table 4-2
Variation of Recovery Factor with discharge for a V-shaped channel with an
annual average flow rate of 10,000 m³/s and a slope of 0.0005.

Flow percentile	Q_5	Q_{25}	Q_{50}	Q_{75}	Q_{95}
Flow rate (m³/s)	1,800	3,400	6,000	11,800	31,800
Recovery Factor	0.28	0.27	0.24	0.21	0.16
Average depth (m) in deployment area *with no* devices.	4.68	6.59	8.80	12.19	19.1
Average depth (m) in deployment area *with* devices.	5.79	7.96	10.40	14.03	21.26
Blockage ratio in deployment area neglecting back effects	0.209	0.148	0.111	0.080	0.051
Blockage ratio in deployment area accounting for back effects	0.169	0.123	0.094	0.070	0.046
Blockage ratio in the river cross-section accounting for back effects	0.147	0.093	0.061	0.038	0.018

The recovery factors for 32 flow and slope scenarios are provided in Table 4.3. The recovery factors in Table 4.3 were estimated based on the recovery factor for the 50-percentile flow. Table 4.3 also displays the average water depth in the deployment area with and without devices at the 50-percentile flow rate for selected scenarios. The data shows that the impact of devices is greatest when the discharge is greatest.

Table 4-3
Discharge - river slope scenarios and recovery factor calculation results. ND= no data.

Annual average flow rate (m^3/s)	Slope	Recovery factor	Average depth (m) in deployment area *with no* devices (at Q_{50})	Average depth (m) in deployment area *with devices* (at Q_{50})
10000	0.001	0.23	ND	ND
3000	0.001	0.17	ND	ND
3000	0.005	0.13	ND	ND
1000	0.005	0	-	-
10000	0.002	0.22	ND	ND
3000	0.002	0.16	ND	ND
1000	0.002	0.07	3.61	3.77
700	0.002	0.03	3.3	3.36
400	0.002	0	-	-
1000	0.001	0.09	4.0	4.23
700	0.001	0.06	3.63	3.79
400	0.001	0	-	-
10000	0.0005	0.24	8.80	10.40
3000	0.0005	0.19	6.04	6.84
1000	0.0005	0.12	4.39	4.74
400	0.0005	0.04	3.45	3.55
200	0.0005	0	-	-
20000	0.0003	0.27	12.14	14.78
10000	0.0003	0.25	9.59	11.42
1000	0.0003	0.14	4.68	5.11
500	0.0003	0.09	3.88	4.10
200	0.0003	0	-	-
20000	0.0001	0.28	14.64	17.67
10000	0.0001	0.27	11.52	14.0
1000	0.0001	0.18	5.52	6.20
200	0.0001	0.04	3.52	3.58
100	0.0001	0	-	-
20000	0.00002	0.24	21.63	25.88
10000	0.00002	0.23	16.96	19.85
3000	0.00002	0.09	11.94	12.38
1000	0.00002	0.02	8.59	8.64
100	0.00002	0	-	-

Based on these data, an expression was developed to relate recovery factor (RF) to annual average flow rate (Q, m³/s) and slope (S):

$$RF = \frac{0.002647(Q-200)^{0.3426}}{\sqrt{62.4277\,S^2}}\; e^{\frac{-(Log(S)-1.498)^2}{19.87}} \qquad if\ Q > 200 \quad Eq.\ 4\text{-}3$$

$$RF = 0 \quad if\ Q \leq 200$$

This expression explains 88% of the variance in recovery factor for the set of scenarios in Table 4.3. Two viewpoints of a surface plot of the RF expression and the data points in Table 4.3 are depicted in Figure 4-2. The expression was used to calculate segment-specific recovery factors and estimate the technically recoverable hydrokinetic energy resource throughout the contiguous 48 states.
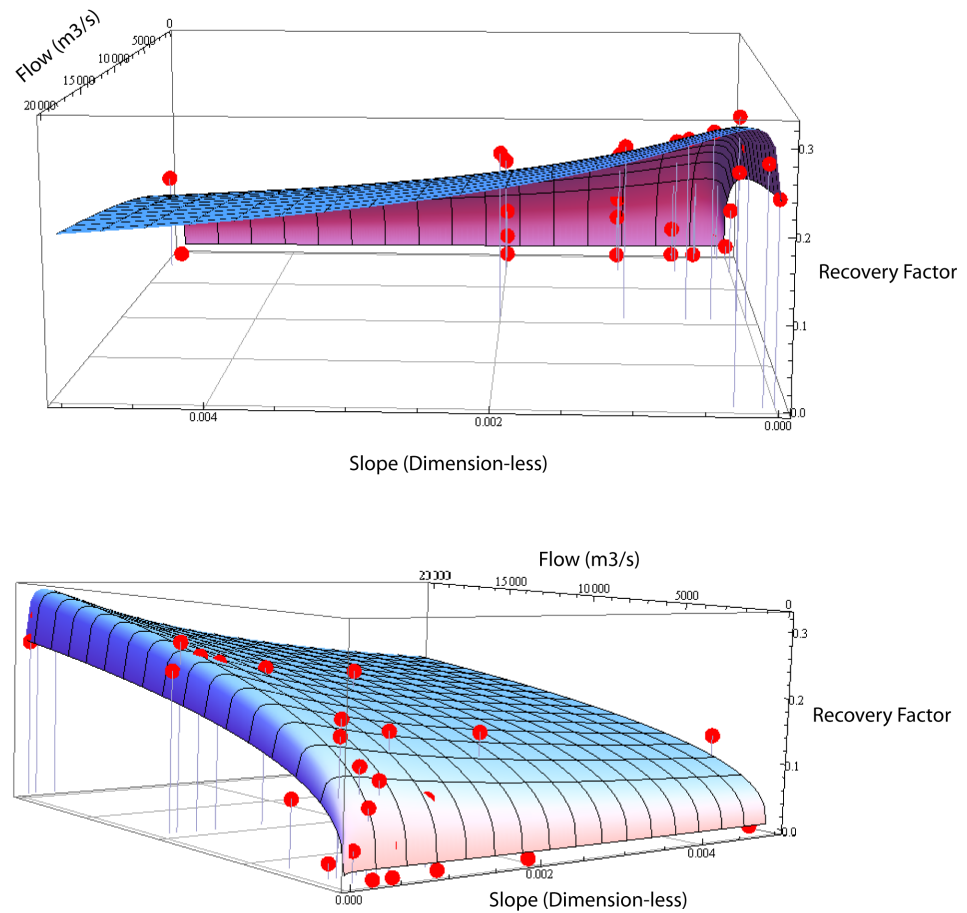
Figure 4-2
Two views of a plot of the Recovery Factor scenario results (data points) listed in Table 4.3 and fitted Recovery Factor function (surface plot).

For Alaska, data on river slope was not readily available. Hence, the Recovery Factor was estimated based on the flow rate alone using:

$$RF = 0.0557\, ln(Q) - 0.2946 \qquad\qquad Eq.\ 4\text{-}4$$

The above equation (with an R^2 of 0.78) was obtained from the Recovery Factor and flow rate data from Table 4.3. The relationship between annual average flow rate and recovery factor is displayed in Figure 4.3 below.
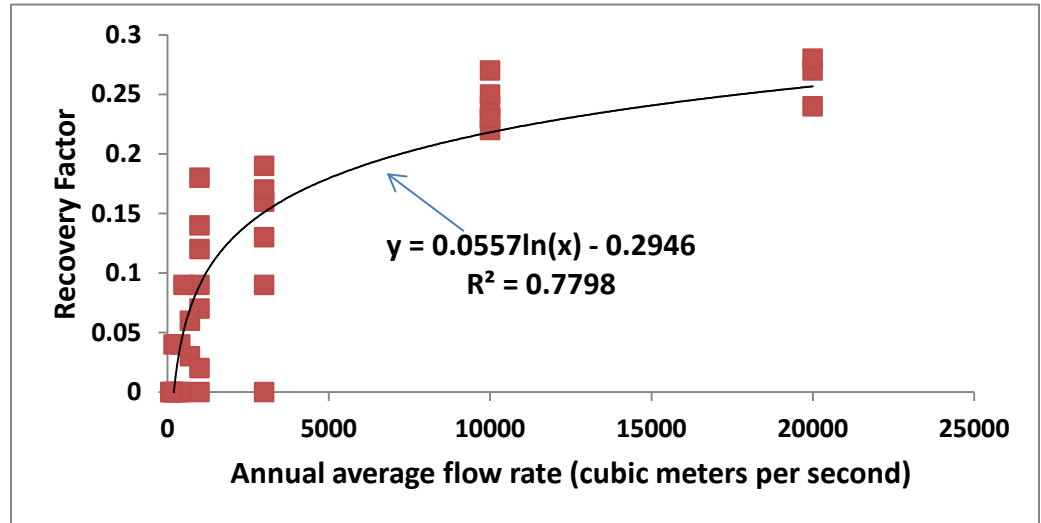
Figure 4-3
Plot showing the relationship between Recovery Factor and discharge based on data in Table 4.3.

This recovery factor function was applied to the discharge data for individual river segments identified in Appendix C to estimate the technically recoverable in-stream hydrokinetic power for those Alaska river segments with average discharge greater than 10,000 cfs.

Section 5: Results for the Technically Recoverable Hydrokinetic Resource

The technically recoverable resource is presented by hydrologic region in Table 5.1. The total estimated technically recoverable power is 120 TWh/yr. The Lower Mississippi region contributes nearly half (47.9%) of the total resource estimate. The major rivers of Alaska constitute 17.1% of the total for the continental U.S. The next largest contributor is the Pacific Northwest region, which contributes 9.2%, followed by the Ohio region (5.7%).   Collectively these four regions encompass 80% of the technically recoverable hydrokinetic resource in the continental U.S.

Table 5-1
Technically recoverable hydrokinetic resource for the continental United States, by hydrologic region depicted in Figure 3.1 and for Alaska.

Hydrologic Region	Technically Recoverable Annual Energy (TWh/yr)	Portion of Total Technically Recoverable Resource (%)
New England	0.2	0.2
Mid Atlantic	1.0	0.8
South Atlantic Gulf	1.2	1.0
Great Lakes	0.01	0.2
Ohio	6.9	5.7
Tennessee	1.0	0.9
Sauris Red-Rainy	0.03	0.03
Upper Mississippi	5.1	4.2
Lower Mississippi	57.4	47.9
Texas Gulf	0.05	0.04
Arkansas Red	1.3	1.0
Lower Missouri	5.6	4.7

Table 5-1 (continued)
Technically recoverable hydrokinetic resource for the continental United States, by hydrologic region depicted in Figure 3.1 and for Alaska.

Hydrologic Region	Technically Recoverable Annual Energy (TWh/yr)	Portion of Total Technically Recoverable Resource (%)
Upper Missouri	2.8	2.3
Rio Grande	0.3	0.2
Lower Colorado	3.9	3.2
Upper Colorado	1.1	0.9
Great Basin	0	0
California	0.7	0.6
Pacific Northwest	11.0	9.2
Alaska	20.5	17.1
Total	**119.9**	

Section 6: Uncertainty of the estimates of the Theoretical and Technically Recoverable Hydrokinetic Resource

Uncertainty in the theoretical resource is directly related to uncertainty in the discharge and in the river slope as is evident in Eq. 1.1. The project team examined uncertainty of the total theoretical resource estimate as well as uncertainty of the theoretical resource estimate in individual river segments. The uncertainty of the overall resource estimate was judged to be relatively small. The team examined river elevation change between the headwaters and the river mouth as represented by NHDPlus and as estimated by an alternative source (Table 6.1). The NHDPlus data was in good agreement with the alternative data so it was judged that river slope uncertainty would not contribute significantly to overall uncertainty in the resource estimate at the scale of entire rivers. For individual segments, however, the percent errors can be larger.

Table 6-1
Uncertainty analysis of river elevation change between headwaters and mouth

River	NHDPlus elevation change (m)	Alternative elevation change (m)	Percent difference	Source of alternative data
Colorado	1714	1734	1%	Google Earth
Missouri	1180	1110	6%	Google Earth and Wikipedia
Snake	1986	1960	1%	Google Earth
Arkansas	1975	2000	1%	Google Earth and Wikipedia

Analysis of NHDPlus and USGS discharge data indicated that uncertainty in NHDPlus discharge data would not contribute to significant uncertainty in the overall theoretical resource estimate. Uncertainty in the NHDPlus discharge (referred to as "MAFLOWU" in the database) was studied by comparing NHDPlus discharge estimates ($Q_{NHDPlus}$) and USGS-gage measurements (Q_{USGS})

at a representative location in each of the 36 hydrologic regions represented in the NHDPlus database (Figure 6.1). The plot of the individual data points (comparing the two estimates) and the linear regression of $Q_{NHDPlus}$ and Q_{USGS} both show that $Q_{NHDPlus}$ is an unbiased estimate of discharge in the river segments – assuming that USGS gage data is reasonably accurate. Note, USGS gage data has an uncertainty of about 10% for a 30 year record (Benson and Carter 1973) . Hence, for the overall theoretical resource estimate, which is essentially the sum of numerous river segment discharge estimates, uncertainty in NHDPlus discharge estimates would not contribute to significant uncertainty in the overall theoretical resource estimate.

However, our analysis indicates that there is significant uncertainty in our estimates of the theoretical resource in individual river segments. In individual segments, both river slope uncertainty and discharge uncertainty contributed significantly to theoretical resource uncertainty. For example, according to NHDPlus documentation (McKay *et al.* 2012), in some instances, it was necessary for the NHDPlus developers to manually smooth the river slope in order to get rivers to flow in the correct direction. There is also significant uncertainty in the NHDPlus discharge in individual river segments. For example, in the data shown in Figure 6.1, the NHDPlus discharge deviated from the USGS measurement by 77% (on average), with some minor over-estimation of discharge (in the NHDPlus estimate) at low flow rates.
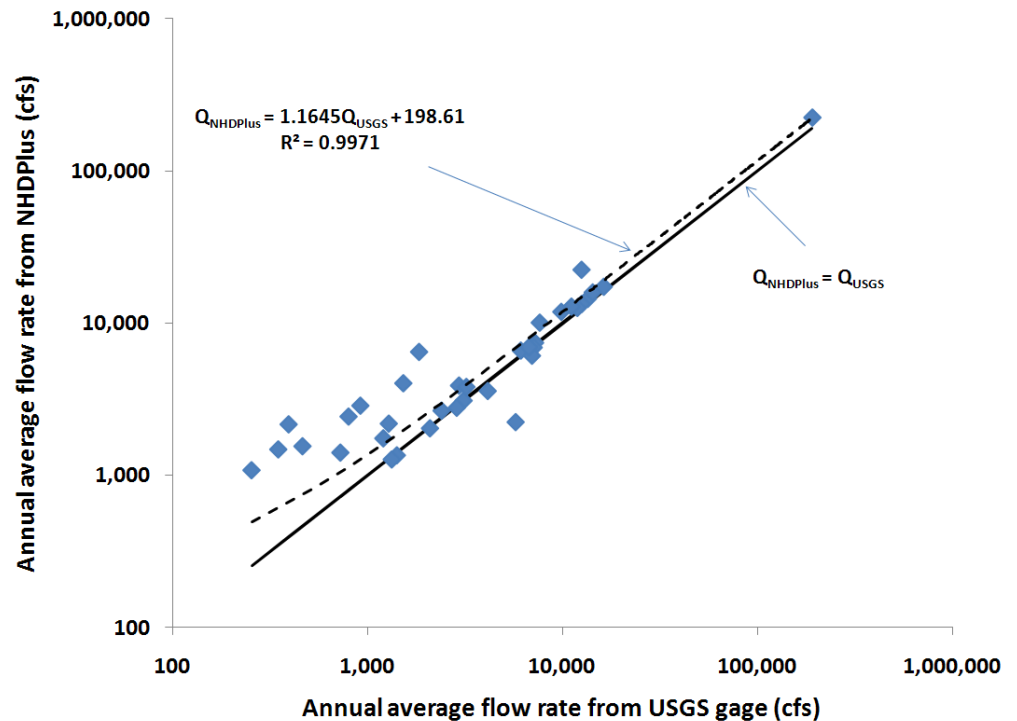
Figure 6-1
Comparison of NHDPlus-estimated discharge and USGS gage measured discharge at selected locations in each of the hydrologic regions of the US.

The uncertainty in the estimation of the recovery factor and technical resource can be studied by examining the methodology used to estimate the recovery factor. As described in $\S0?494$, an expression for the recovery factor as a function of average discharge and as a function of river slope was developed based on a "case studies" approach. The case studies assumed a "V" – shaped channel profile with a side slope of 0.06 and it assumed normalized flow distribution curve based on flow statistics from the Mississippi River at Vicksburg Mississippi. In order to estimate the uncertainty in the recovery factor (and technical hydrokinetic resource), a number of sensitivity studies were done. These studies included:

1. A comparison of the recovery factor calculated for an idealized V-shaped channel (side slope = 0.021) with that for a real channel with the same average side slope.

2. A comparison of the recovery factor calculated for an idealized V-shaped channel with a side slope of 0.06 with that calculated for side slopes of 0.03 and 0.09 (using the case shown in Table 4.2 as a baseline).

3. A comparison of the recovery factor calculated assuming in-row spacing of 2D between devices with a spacing of 1D between devices.

4. A comparison of the recovery factor calculated assuming $Q_5/Q_{ave} = 0.18$ (Table 4.1) with the recovery factor calculated assuming $Q_5/Q_{ave} = 0.35$.

5. A comparison of the recovery factor calculated assuming a Manning roughness coefficient of 0.025 instead of 0.03.

A summary table presenting the sensitivity of Recovery Factor to effects 1 through 5 above is provided in Table 6.2 below. The sensitivity study indicates that the recovery factor for a given river segment is uncertain. Since the recovery factor and the theoretical resource in a given segment are uncertain to a large degree, it is clear that technical resource in a given segment is also quite uncertain. We can next turn our attention to the uncertainty of the overall technical resource estimate. Earlier, we argued that the estimate of the overall theoretical resource is fairly certain since there was no significant source of bias in the theoretical estimates in individual river segments. Here, we again argue that the overall theoretical resource is fairly certain since there are no significant sources of bias in the recovery factor. A potential source of bias (on the order of 16%) is the bias in NHDPlus flow rates relative to USGS gage measurements.

Table 6-2
Sensitivity of Recovery Factor calculation

Sensitivity test	Sensitivity (% change from baseline)
Use real river profiles instead of "V" shape	15%
Use of side slope of .03 or 0.09 instead of .06	-9%, 9%
Device spacing of 1D (not 2D) in rows	-4%
Q_5/Q_{ave} = .35 instead of .18	16%
Manning roughness of 0.025 instead of 0.03	4%

More insight into sources of uncertainty in this project is obtained by examining the NHDPlus database in more detail. Though NHDPlus is the best dataset for a project of this scope, it is important to note its limitations. Also NHDPlus does not exist for the State of Alaska which requires a different approach. A more detailed description of NHDPlus is at http://www.horizon-systems.com/NHDPlus/data/NHDPLUS_UserGuide.pdf

The user of these data should be aware that while these data can be used to obtain a useful estimate of the hydrokinetic resource in the contiguous 48 states, as well as the broad scale distribution of the resource, the data are not suitable for identifying sites suitable for hydrokinetic project deployments.

Section 7: GIS Display

The geo-spatial results of this assessment are available as an interactive web-based Geographic Information System (GIS) application called the River Atlas app. The River Atlas is deployed using the National Renewable Energy Laboratory's (NREL's) OpenCarto framework. OpenCarto is an open architecture framework that utilizes open source libraries (e.g., MapServer, TileCache, Ext-JS and OpenLayers), and standards such as Styled Layer Descriptor (SLD), Web Mapping Service (WMS) and Web Feature Service (WFS). OpenCarto is designed to support analysis, visualization and data exploration, and is an ideal medium for the visual representation of the riverine hydrokinetic data. Currently, results are only available for the 48 contiguous states. Results will be made available for Alaska in the future.

Data Processing

NREL received the data as GIS shapefiles along with a MXD file. The shapefiles contain the data variables and georeferenced coordinates. The MXD file was used as a reference for styling the visual representation of the data within the stand-alone application.

The shapefiles were re-projected in the WGS_1984 Geographic Coordinate System for compatibility with the OpenCarto framework. The re-projected data were then converted from shapefiles to a PostGIS object relational database.

OpenCarto can access the data from the spatial database repository, and by creating unique layers for each data variable the hydrokinetic data can be rendered in a web mapping application. The river networks are displayed as line segments reflecting the power variable in the database and classed by standard deviation. Unique layers were created for three power classes (low, medium, and high). By default, the layers are generated as simple spatial geometries with no associated style. Applied rules give each power class a line color and stroke width.

Tool Functionality and Capabilities

The River Atlas app is a web-based application that was selected as the tool to visually display the riverine hydrokinetic resource data; it is a specific application module that is hosted on the OpenCarto platform. The data are displayed by adding the layers to the application module. The river app was assigned a URL (**http://maps.nrel.gov/river_atlas**) to allow users to access and interact with the

data. The basic components of the application are a map window for displaying the data, a content display window (which uses tabs to display the map layers, legend, and data sources), and a toolbar.

The River Atlas app has additional capabilities that allow the user to interact with the data and create customized visualizations and maps. The query tool provides several options that return query results from the spatial database. The data can be queried by point, region, or attribute. The query will return results from the geometry feature(s) in a new window and also highlight the selected feature(s) on the map. Region query results can be downloaded by the user as a CSV file.

OpenCarto capabilities allow users to generate their own thematic maps. The layer tree can be customized to reorder the layer index, class thresholding can be performed to display only the data of specific interest to the user, and legend and class display colors can be customized. Data results can be downloaded and customized maps can be printed if desired.

Application Analysis

The interactive capabilities of the application can be used for basic data analysis on active layers. Results for specific, user-selected geographic points or regions can be returned using the query tool. The query results can be coupled with other layers to obtain answers to questions such as estimating the resource potential in a specific county or state.

A combination of capabilities and tools can also be used to determine distance from a specified river segment. By using layer thresholding, a user can display only power values within specified numerical bounds. Then, using the measure tool, a distance from those river segments to the nearest point of interest (e.g., city or known transmission line) can be estimated.

The flexibility of the application and customization of the data allows users to perform basic analysis, and with the capability of downloading the data users can perform their own advanced analysis and modeling.

Intended Audience

The mission of DOE's Water Power Program is to perform and sponsor the necessary research, development, testing, evaluation and demonstration of innovative water power technologies leading to cost-effective environmentally responsible generation of renewable energy, including from marine and hydrokinetic (MHK) resources.

The River Atlas app is a tool that supports attainment of this goal by providing an easy-to-use interactive visual interface. This type of interface is beneficial both to audiences who may be familiar with marine and hydrokinetic resources, and also to those who are exploring them for the first time.

The application can deliver insight and facilitate discovery of geographic regions and riverine systems with relatively high hydrokinetic resources. While the application and supporting data are not suitable for siting studies, they may help researchers and others identify rivers meriting more in-depth data collection and siting studies.

Section 8: Conclusions

An information base exists from which the theoretically available and technically recoverable riverine, hydrokinetic resource can be estimated for the continental United States. These data were used to make such an assessment utilizing established hydraulic engineering principles and advice from relevant experts. The resulting assessment substantially advances understanding of the hydrokinetic resource potential in the continental United States. The more detailed and comprehensive assessment reported here yields an estimate of technically recoverable hydrokinetic energy (119.9 TWh/yr) that is approximately 9% greater than the estimate from the only other nationwide assessment (i.e., Miller *et al.* 1986). A difference of this magnitude is not unexpected given the differences in criteria for waterbody inclusion and differences in analytical methodology. Large differences between the two studies in regional distribution of the resource can be attributed to differences in methodology as well.

The data gathering and reporting programs supplying the data, however, were not designed and implemented with hydrokinetic resource assessment as an intended application of the data. Furthermore, operating riverine hydrokinetic projects don't yet exist to provide a means of validating important assumptions incorporated into this assessment. Consequently, the assessment substantially advances understanding of the hydrokinetic resource potential of the United States; however, substantial uncertainty remains. Uncertainty and error are greatest at the scale of individual segments, and results are not appropriate for siting projects or ranking river segments. Further work is needed to develop and validate models of the hydraulic effects of hydrokinetic turbine projects. Such modeling tools are needed for refined resource assessment, project planning, and environmental impact assessment.

Improved understanding also is needed of the practical constraints on development of the hydrokinetic resource and of the impact of those constraints on the portion of the technically recoverable resource that may ultimately be exploited. Significant improvements in understanding of the hydrokinetic resource will require more detailed hydrologic information, site-specific information on constraints imposed by existing uses and environmental sensitivities, and empirical validation and refinement of hydrokinetic array models. Given the uncertainties that currently exist, the practical resource is an unknown fraction of the technically recoverable resource estimated by this study.

Appendix A: Validation

The National Renewable Energy Laboratory's validation of the hydrokinetic energy resource values in the GIS database was different from NREL's previous validations of wind and wave power estimates. Due to the scarcity of complete stream-flow and channel cross-section information, all available information was used to help compute the in-stream resource, meaning that these data can no longer serve as an independent data set for validation. Moreover, we know of no direct measurements of in-stream energy that could be used to validate the model.

Consequently, NREL's validation effort was limited to the inspection of the estimated resource values to verify that they are reasonable, consistent over time, reproducible, and were within the statistical bounds of other naturally varying river systems.

The primary validation process consisted of a statistical analysis of the individual river segments and their contribution to the total resource. Segments were grouped by power output, power per km, slope, flow and other measures, and the largest values in each group were inspected manually. GoogleEarth was used to determine whether high power values were caused by actual high-gradient regions or by dams that had slipped through the automated dam identification process. Segments were also grouped by river, and obvious outliers were removed. This power screening process also identified a few segments at the US-Canada border that had erroneous values of delta-h.

After removal of all anomalous segments, the remaining segments were sorted by power. The top 10 most powerful segments were all located on the Mississippi River. Almost two-thirds of the top 150 segments were on the Mississippi, followed by the Colorado, Ohio, Missouri and Columbia Rivers. A final ranking of the top power producing rivers is shown in Table A-1.

Table A-1
Top Rivers by Power Production

River	Theoretical Power (TWh/yr)
Mississippi River	217.3
Colorado River	79.2
Missouri River	59.8
Snake River	41.7
Ohio River	40.5
Arkansas River	29.8
Rio Grande	28.5
Yellowstone River	26.4
Columbia River	26.3
Salmon River	22.6

The general order shown in this table is roughly what one would expect. The high value for the Snake River is due to a few segments with high delta-h, but these may be in error. Some high powers from the Colorado and Yellowstone Rivers are from rapids and/or waterfalls. These features are often located in national parks or other protected sites and would be removed from consideration if a complete database of environmental exclusions were applied.

As riverine hydrokinetic project siting studies and deployments accrue, data suitable for further model refinement and validation will become available.

Appendix B: Hydraulic Impacts of Hydrokinetic Devices

Abstract

A simple technique to estimate the far-field hydraulic impacts associated with the deployment of hydrokinetic devices is introduced. The technique involves representing the presence of hydrokinetic devices as enhanced bottom roughness. The enhanced Manning roughness is found to be a function of the Manning roughness of the natural channel, device efficiency, blockage ratio, density of device deployment and water depth. The technique is developed assuming simple, open channel flow geometry. However, once the effective bottom roughness is determined, it can be used to determine the hydraulic impact of arbitrary device configurations and arbitrary flow situations.

Introduction

Hydrokinetic energy conversion devices are deployed in flowing water, and they extract energy according to the kinetic energy or velocity of the flowing water. The power available from hydrokinetic devices, per unit swept area, is termed the hydrokinetic power density (PD, W m^{-2}). Hydrokinetic power density is a function of fluid velocity (V, m s^{-1}), fluid density (ρ, kg m^{-3}), and device efficiency (ξ):

$$PD = \xi \, \frac{\rho}{2} V^3 \qquad\qquad Eq. \ B\text{-}1$$

However, as hydrokinetic (HK) devices extract power from flowing water, they can alter the flow velocity, water elevation, sediment transport and other river properties and processes. The goal is to develop simple ways of estimating and representing the far-field hydraulic impacts of HK device deployments. In particular, we develop a technique for representing the presence of hydrokinetic devices with an enhanced bottom roughness. The enhanced bottom roughness can be used in standard hydraulic calculation procedures and models to determine the device impact.

A widely-used open channel flow equation for relating flow velocity (or discharge) to bottom roughness and channel properties is the Manning Equation. Here, the equation is presented in two forms:

$$V = \frac{1}{n} R^{2/3} S^{1/2} \quad or \quad Q = \frac{A}{n} R^{2/3} S^{1/2}$$

<div align="right">Eq. B-2</div>

where V is the cross-section averaged velocity (m s^{-1}), n is the Manning roughness coefficient (m$^{-1/3}$ s), R is the hydraulic radius (cross-sectional area/wetted perimeter, m), S is the slope, Q is the discharge (m^3 s^{-1}), and A (m^2) is the cross-sectional area. Note, the second version of the Manning Equation is obtained from the first version through application of the continuity principle (Q =VA). Since HK devices tend to impede the flow of water, they can be represented with an enhanced bottom roughness, n_t. According to the Manning Equation, all other parameters being unchanged, an enhanced bottom roughness would cause a reduction in velocity. In a river setting, where the discharge can be considered constant, the reduced velocity will be compensated for with an increase in water depth.

The majority of previous work on the interaction of hydrokinetic devices and flowing water focused on the calculation of the available hydrokinetic power in tidal systems (Garrett and Cummins 2005, Bryden and Couch 2006, Sutherland *et al.* 2007, Garrett and Cummins 2008, Karsten *et al.* 2008, Polagye 2009). In tidal systems, often conceptualized as a channel connecting two basins – one semi-infinite and one finite – the central question is: what fraction of the total energy passing through the tidal channel is available for HK extraction? The researchers found that as the number of hydrokinetic devices increased, the flow rate of water through the channel decreased. Further, as the number of devices increased, there was a peak in total energy extraction followed by a decline.

Researchers (e.g., Garrett and Cummins 2007, Garrett and Cummins 2008) have also addressed the question of the relationship between the power extracted by hydrokinetic devices ($P_{extraction}$) and the total power dissipated by the presence of the devices ($P_{dissipation}$). The power extracted by hydrokinetic devices is the product of the power density (PD) and the swept area of the devices. Focusing on a single device in a channel, they noted that the devices generated a low velocity zone in their wake. Further, when the low water velocity wake mixed with the high velocity water that flowed around the device, significant energy was dissipated. Garrett and Cummins (2007, 2008) report:

$$\frac{P_{extraction}}{P_{dissipation}} = \frac{2}{3(1+\varepsilon)}$$

<div align="right">Eq. B-3</div>

where   is the blockage coefficient (i.e., the fraction of the river cross-sectional area occupied by the HK device). In this formulation, $P_{dissipation}$ is the total power dissipated in a stretch of river. It is assumed that there are negligible drag losses.

Analysis

Here, we derive an expression for an enhanced or effective Manning roughness coefficient (n_t) that can be used to represent the presence of hydrokinetic devices. The expression is obtained by considering the conservation of energy equation in two simple flow situations – Case A and Case B. Case A is a wide open channel flow situation in which the flow is steady and uniform. In Case B, hydrokinetic devices have been deployed such that they are distributed uniformly throughout the channel bottom. The channel in Case B is otherwise identical to the one in

Case A. An expression for an enhanced Manning roughness that accounts for the presence of devices is readily determined by assuming that the total flow rate is the same in both situations.

Representation of hydrokinetic devices with an enhanced bottom roughness

Case A – uniform open channel flow with no hydrokinetic devices

Assuming flow from Location 1 to Location 2, the energy conservation equation (or modified Bernoulli Equation) for Case A (no devices) can be written (Munson *et al.* 2002):

$$\frac{P_1}{\gamma} + \frac{V_1^2}{2g} + z_1 = \frac{P_2}{\gamma} + \frac{V_2^2}{2g} + z_2 + h_L \qquad Eq. \ B\text{-}4$$

where P_1 and P_2 are the pressures (Pa) at locations 1 and 2, respectively,

V_1 and V_2 are the velocities (m s^{-1}) at locations 1 and 2, respectively,

z_1 and z_2 are the elevations (m) at locations 1 and 2, respectively,

γ is specific weight (N m^{-3}),

g is acceleration due to gravity (9.8 m s^{-2}), and

h_L is head loss (m) due to bottom friction.

Since flow is uniform in the direction of flow, the pressure and velocity terms cancel out and the energy equation can be written:

$$z_1 - z_2 = \Delta z = h_L \qquad Eq. \ B\text{-}5$$

Further, recognizing that, for uniform flow, the bottom slope is the ratio of the head loss to the length of the channel section (i.e., S = h_L/L), Manning's Equation (Eq. B.2) can be rearranged to obtain head loss in terms of the flow rate, Manning's roughness, channel cross section area (A, m^2), and hydraulic radius (R, m):

$$h_L = \Delta z = \left(\frac{Qn}{AR^{\frac{2}{3}}}\right)^2 L \qquad Eq. \ B\text{-}6$$

Case B – uniform open channel flow with uniform distribution of hydrokinetic devices

In Case B, the channel of Case A is altered to include hydrokinetic devices (i.e., turbines) that are distributed uniformly on the channel bottom. Water pressure (P_{1t} and P_{2t}) and flow velocity (V_{1t} and V_{2t}) differ from that seen in Case A due to the turbine presence. However, variables such as discharge, channel width, and bottom slope remain the same. The energy conservation equation for Case B has the following form:

$$\frac{P_{1t}}{\gamma} + \frac{V_{1t}^2}{2g} + z_1 = \frac{P_{2t}}{\gamma} + \frac{V_{2t}^2}{2g} + z_2 + h_{Lt} + h_p \qquad \text{Eq. B-7}$$

where h_{Lt} is the head loss due to the bottom friction (i.e., contact of the flowing water with the "natural" channel bottom) and h_p is the "head loss" associated with the presence of the hydrokinetic devices (described below).

Since the turbines are uniformly distributed, flow conditions continue to be uniform in the direction of flow. Consequently, upstream and downstream velocity and pressure heads are the same and Equation B.7 can be simplified to:

$$z_1 - z_2 = \Delta z = h_{L\,t} + h_p \qquad \text{Eq. B-8}$$

Using the same approach as for Equation B.5, the head loss associated with bottom friction can be expressed:

$$h_{L\,t} = \left(\frac{Qn}{A_t R_t^{\frac{2}{3}}} \right)^2 L \qquad \text{Eq. B-9}$$

where A_t and R_t are the cross-sectional area and hydraulic radius of the channel when turbines are present. Since the channel geometry in the two cases is the same, Equation B.8 can be written using Equations B.7 and B.9 obtaining:

$$\left(\frac{Qn}{A R^{\frac{2}{3}}} \right)^2 L = \left(\frac{Qn}{A_t R_t^{\frac{2}{3}}} \right)^2 L + h_p \qquad \text{Eq. B-10}$$

Assuming a very wide rectangular channel such that the hydraulic radius is the water depth and the cross-sectional area is the product of the width and depth, Equation B.10 becomes:

$$\left(\frac{Qn}{w h^{\frac{5}{3}}} \right)^2 L = \left(\frac{Qn}{w h_t^{\frac{5}{3}}} \right)^2 L + h_p \qquad \text{Eq. B-11}$$

where h_t is the water depth with devices present.

Channel energy losses due to presence of hydrokinetic devices

Assuming drag losses to be negligible (following Polagye (2009)), the total power dissipated can be estimated based on the blockage area and extracted power as described in Equation B.3. The total power dissipation can be expressed as a "head loss" (i.e., as h_p) by dividing by the product of discharge and the specific weight (i.e., $\gamma\,Q$) obtaining:

$$h_p = \frac{P_{\text{dissipation}}}{\gamma Q} = \frac{3}{4} \frac{\rho N A_r V_t^3}{\gamma\,Q} (\xi\,(1+\epsilon)) = \left(\frac{3}{4} \frac{N A_r Q^2}{g w^3} \cdot \xi\,(1+\epsilon) \right) \cdot \frac{1}{h_t^3}$$

$$\text{Eq. B-12}$$

where   N is the number of hydrokinetic devices in the channel segment,

A$_r$ is the swept area of an individual hydrokinetic device (m^2),

V$_t$ is the cross-section averaged velocity with devices present (m s^{-1}),

w is the channel width (m), and

h$_t$ is the channel depth with devices present (m^2).

Determination of water depth with devices present

Using the expression for "head loss" due to the presence of hydrokinetic devices (Equation B.12), Equation B.11 can be rearranged obtaining:

$$h^{-10/3} - h_t^{-10/3} - \left(\frac{3}{4}\frac{\xi(1+\epsilon)}{n^2 g} \cdot \frac{NA_r}{wL}\right) \cdot h_t^{-3} = 0 \qquad\qquad \textit{Eq. B-13}$$

From Equation B.13, it is apparent that the increased depth associated with the deployment of hydrokinetic devices (h$_t$) can be determined from the character of the channel and the character and number of the devices. Through the principle of continuity, the cross-section averaged velocity can also be determined. Equation B.13 was rearranged obtaining:

$$x^3 - x^{-\frac{1}{3}} - a = 0 \qquad\qquad \textit{Eq. B-14}$$

where $x = \frac{h_t}{h}$ and a $= \left(\frac{3}{4}\frac{\xi\,(1+\epsilon)}{n^2 g} \cdot \frac{NA_r}{wL}\right) \cdot h^{1/3}$.

Next, Equation B.14 was approximated by a cubic polynomial (using MATLAB):

$$1.0849 \cdot x^3 - 0.45336 \cdot x^2 + 0.98303 \cdot x - 1.6145 - a = 0 \qquad \textit{Eq. B-15}$$

The cubic polynomial was solved (for x) and the solution was used to determine the following relationship between *h$_t$*, *h*, and *a*:

$$h_t = h \cdot \left(b^{1/3} - 0.28263 \cdot b^{-1/3} + 0.139296\right) \qquad\qquad \textit{Eq. B-16}$$

where:

$$b = 0.46088 \cdot a + ((0.46088 \cdot a + 0.68368)^2 + 0.022578)^{1/2} + 0.68368$$

For values of x ranging from 1 to 1.5, and for *a* ranging from 0 to 2.50142, the cubic polynomial approximation was found to generate estimates of x (or $\frac{h_t}{h}$) that were very accurate (within 10^{-3} percent). Equation B.16 demonstrates that the hydraulic impacts of a uniform distribution of hydrokinetic devices can be estimated based on a single parameter (parameter *a*, Eq. B.14).

Determination of the effective Manning's roughness coefficient and velocity with devices present

Having determined h_t/h as a function of parameter a, the enhanced Manning roughness coefficient representing the presence of the hydrokinetic devices (i.e., turbines) can be readily determined. Since the discharge and slope under Case A and B are the same, the Manning Equation (Equation 2) can be used to establish a relationship between h, h_t, n, and n_t:

$$\frac{wh}{n} h^{\frac{2}{3}} = \frac{wh_t}{n_t}(h_t)^{\frac{2}{3}} \qquad\qquad Eq.\ B\text{-}17$$

Solving for n_t, we have:

$$n_t = \left(\frac{h_t}{h}\right)^{5/3} \cdot n \qquad\qquad Eq.\ B\text{-}18$$

Based on the continuity principle, the velocity with devices present (V_t m s^{-1}) can also be determined based on h_t/h or n_t/n:

$$V_t = \left(\frac{h}{h_t}\right) V = \left(\frac{n}{n_t}\right)^{3/5} V \qquad\qquad Eq.\ B\text{-}19$$

Example calculation of the hydraulic impact of a uniform distribution of hydrokinetic devices

In order to illustrate the technique for estimating the hydraulic impact of hydrokinetic devices, a set of channel, flow, and hydrokinetic device properties were assumed (Table B.1). Further, it was assumed that the hydrokinetic devices were deployed in rows (normal to the flow) separated by 10 device diameters (i.e., 10 D or 80 m). Given the properties in Table B.1, it is clear that we were modeling a single row of devices with the roughness of the devices distributed throughout the channel length. Then, assuming an increasing number of devices per row (or number of devices in the 80 m long channel segment), the impact of the devices on the normalized depth (h_t/h), normalized effective bottom roughness (n_t/n), and normalized velocity (V_t/V) were calculated based on Equations B.16, B.18, and B.19, respectively as a function of the number of devices per row (or per 10 D of channel length). (Figure B.1). In this example, the maximum number of devices per row was capped at 20. This amounts to spacing between devices of 17.9 m or 2.2 D. This spacing is approximately equal to 2D, which is often considered an upper density limit.

Table B-1
Channel, flow, and turbine properties assumed in example calculation.

Variable	Symbol	Value
water depth	h	10 m
channel width	w	500 m
channel length	L	80 m
Slope	S	0.0002
Manning roughness	n	0.025
turbine efficiency	ξ	32%
turbine swept area	A_r	51 m^2

Figure B.1 also shows the blockage ratio (ϵ), power density, and total power (for a 80 m long channel) as a function of density of hydrokinetic devices (i.e., number of devices per row). It is noteworthy that the normalized depth, Manning roughness, and velocity all start at a value of 1.0 on the left side of the plot (where the device density is 0). As the density of devices increases, the normalized depth and Manning roughness monotonically increase whereas the normalized velocity decreases. Initially, the total extracted power increases rapidly. Later, there are diminishing returns in extracted power with incremental increases of device density. This is because the water has been slowed by the devices that have already been deployed in the channel. The diminishing energy level of the channel with increasing device density is shown by the power density curve which decreases rapidly with increasing numbers of devices.
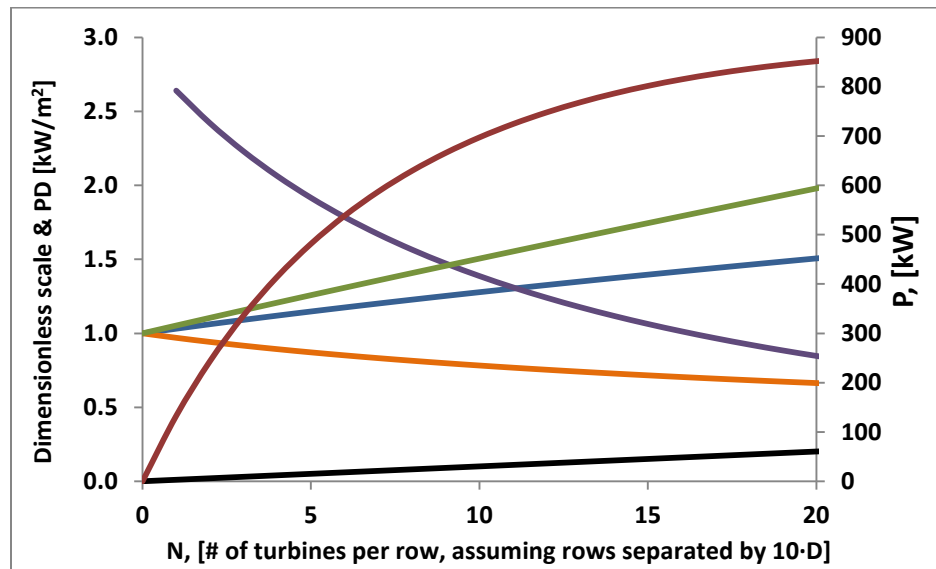

Figure B-1
Plot of normalized depth (h_r/h ▬), normalized velocity (V_r/V ▬), normalized effective Manning roughness (n_r/n ▬), power density (PD, kW m^{-2} ▬), extracted power in a 500-m long channel section (P, kW ▬), and blockage ratio (▬)as a function of density of hydrokinetic devices (number of devices per 10 D m length).

The blockage ratio plotted in Figure B.1 and used in equation B.14 is based on the water depth in a device-free channel (h). That is, the calculations of blockage ratio presented here do not account for the depth increase due to the presence of HK devices. Calculations show that including these "back effects" in the blockage ratio has a negligible effect on water level. For example, for the situation shown in Figure B.1, if the back effect is accounted for the h_t/h ratio at 20 devices per row would decrease from 1.506 to 1.486, , change $\mathbf{F}\ \mathbf{Ek}^{'}$.

Hydraulic impacts of HK devices associated with deployments in spatially limited areas

The previous section indicated that a uniform distribution of hydrokinetic devices can have a significant impact on water level and velocity. In order to determine the impact of hydrokinetic devices when they are deployed in limited areas, a 1D numerical model (ISIS) was employed. To illustrate the impact of different spatial extents of hydrokinetic device deployments, a single device density (27 devices per 500 m segment or 4.5 per 80 m segment) and the same channel geometry was assumed (Table B.2). However, the longitudinal extent of the deployment was limited to just 500 m (Figure B.2). In this case the water level and velocity impact was significantly reduced relative to the impacts obtained if the device deployment was unlimited in the longitudinal direction (Figure B.3). Specifically, the enhancement in water level was only about 6 cm instead of about 1.1 m.

Table B-2
Channel, flow and turbine properties assumed.

Variable	Symbol	Value
water depth	h	10 m
channel width	w	500 m
Slope	S	0.0002
Manning roughness (no devices)	n	0.025
turbine efficiency	ξ	32%
turbine swept area	A_r	51 m^2
Manning roughness (18 devices per 100 m Segment)	n_t	0.0308
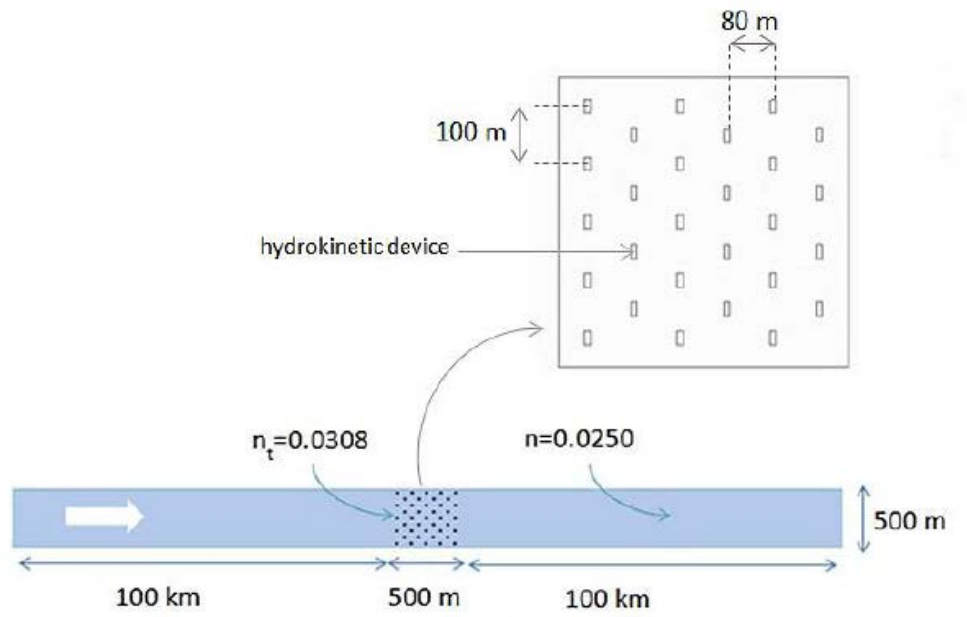
Figure B-2
Cartoon illustrating the spatially limited deployment of hydrokinetic devices.
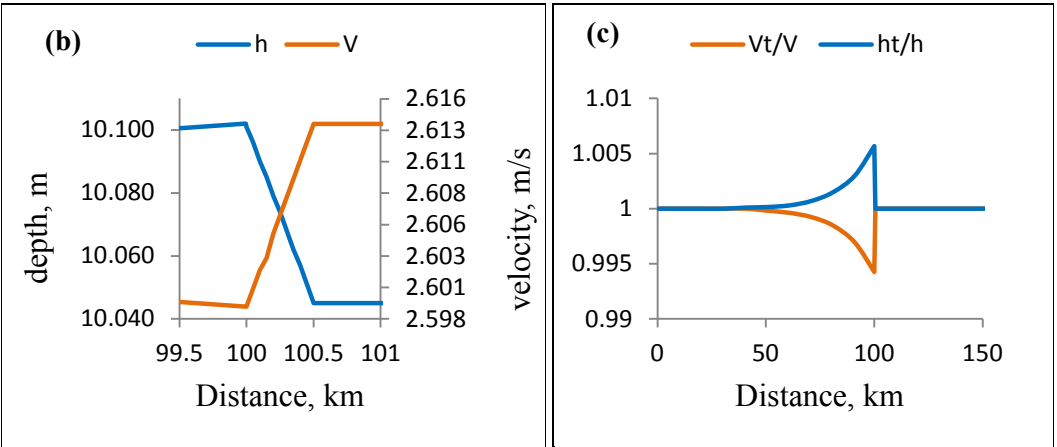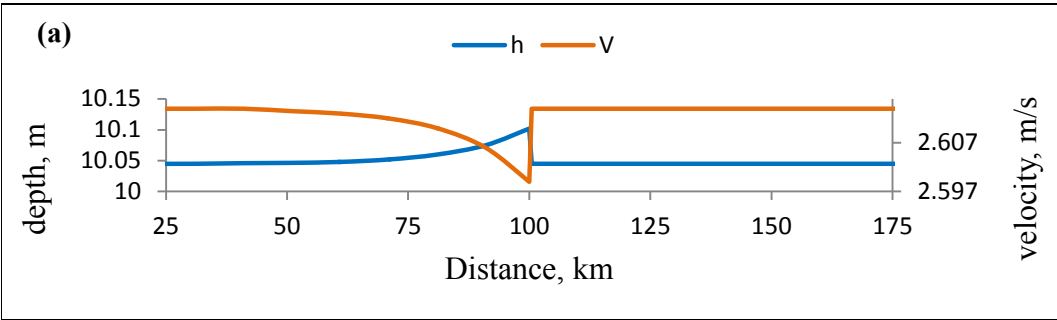
Figure B-3
Hydraulic impact of a spatially-limited deployment of hydrokinetic devices
including (a) velocity and water depth within 75 km of the hydrokinetic devices;
(b) Velocity and water depth within 0.5 km of the devices; and (c) normalized
velocity and normalized depth proximal to the devices.

Notation

A cross sectional area of the channel (m²)

A_t cross sectional area of the channel for the case when turbines are uniformly distributed over the bottom (m²)

A_r cross sectional area of the rotor for one turbine unit (m²)

C_d drag coefficient

F_d drag force (N)

g acceleration due to gravity (9.81 m/s²)

h water depth (m)

h_E head loss due to due to power extraction (m)

h_{FD} head loss due to due to the drag force for one turbine unit (m)

h_{Lt} head loss due to bottom fiction the case when turbines are uniformly distributed over the bottom (m)

h_L head loss due to bottom fiction (m)

h_p head loss due to turbines operation, caused by power production and drag forces acting on the turbines (m)

h_t water depth for the case when turbines are uniformly distributed over the bottom (m)

L   channel length (m)

$\dot{m}$ mass flow rate (kg/s)

n Manning's roughness coefficient

n_t effective Manning's roughness coefficient that is attributed to placing turbines

$P_{1,2}$ pressure at the point (N/m²)

ρ fluid density (1000 kg/m³)

Q volume flow rate (m³/s)

R hydraulic radius (m)

R_t hydraulic radius for case when turbines are uniformly distributed over the bottom (m)

S slope of the channel (m/m)

Un velocity ratio (or tip speed ratio)

V average fluid flow velocity in the channel (m/s)

$V_{1,2}$ fluid flow velocity at a point on a streamline (m/s)

$\dot{W}$ power (Watts)

w channel width (m)

$z_{1,2}$ elevation of the point above a reference plane (m)

Δz elevation change over the channel length (m)

γ specific weight (N/m^3)

ξ turbine efficiency

ε blockage ratio

σ turbine solidity

Appendix C: Theoretical and Technically Recoverable Riverine Hydrokinetic Power in Alaska

The theoretical resource was estimated for the segments of major Alaska rivers with average discharge greater than 10,000 cfs. These river segments and their associated theoretical power are listed in Table C-1.

Table C-1
Theoretical in-stream hydrokinetic power in segments of the major Alaska rivers in which the annual average flow rate exceeds 10,000 cfs (283 m³/s).

River	Segment start	Segment end	Q_{ave} (m³/s)	ΔH (m)	Power (MW)	Power (TWh/yr)
Yukon	Kaltag	Pilot Station	6284	30.2	1858.8	16.3
	Ruby	Kaltag	5413	13.1	695.4	6.1
	Stevens Village	Ruby	4031	47.9	1891.0	16.6
	Eagle	Stevens Village	2876	168.3	4743.9	41.6
					TOTAL:	80.5
Koyukuk	Hughes	Koyukuk	575	50.0	281.9	2.5
	66° 34' N, 152° 38' W	Hughes	408	30.8	123.1	1.1
	66° 49' N, 151° 47' W	66° 34' N, 152° 38' W	282	43.9	121.3	1.1
					TOTAL:	4.6
Tanana	Fairbanks	Nenana	621	28.4	172.4	1.5
	Big Delta	Fairbanks	485	163.7	777.5	6.8
	Tok Junction	Big Delta	300	452.4	1331.9	11.7
					TOTAL:	20.0
Kuskokwim	Chuathbaluk	Bethel	1773	26.8	466.2	4.1
	Crooked Creek	Chuathbaluk	1415	14.3	198.7	1.7
	Stony River	Crooked Creek	1120	19.8	217.5	1.9
	62° 23' N, 156° 0' W	Stony River	854	23.2	193.8	1.7
	62°47' N, 155° 45' W	62° 23' N, 156° 0' W	632	14.9	92.5	0.8
	63° 0' N, 154° 54' W	62°47' N, 155° 45' W	446	7.9	34.7	0.3
					TOTAL:	10.5

Table C-1 (continued)
Theoretical in-stream hydrokinetic power in segments of the major Alaska rivers in which the annual average flow rate exceeds 10,000 cfs (283 m³/s).

River	Segment start	Segment end	Q_{ave} (m³/s)	ΔH (m)	Power (MW)	Power (TWh/yr)
Stikine	56° 40′ N, 132° 7′ W	Coast	3863	0.8	31.2	0.3
	56° 42′ N, 132° 0′ W	56° 40′ N, 132° 7′ W	3843	2.5	93.0	0.8
	56° 93′ N, 131° 51′ W	56° 42′ N, 132° 0′ W	3816	3.7	139.1	1.2
					TOTAL:	2.3
Kvichak	59° 12′ N, 156° 26′ W	Coast	738	10.1	72.8	0.6
	59° 15′ N, 156° 5′ W	59° 12′ N, 156° 26′ W	723	3.7	25.9	0.2
	59° 20′ N, 155° 54′ W	59° 15′ N, 156° 5′ W	699	1.6	10.6	0.1
					TOTAL:	0.9
Nushagak	58° 52′ N, 157° 50′ W	Coast	827	3.1	25.0	0.2
	59° 2′ N, 157° 46′ W	58° 52′ N, 157° 50′ W	823	5.5	44.5	0.4
	59° 18′ N, 157° 34′ W	59° 2′ N, 157° 46′ W	772	6.9	52.5	0.5
	59° 25′ N, 157° 19′ W	59° 18′ N, 157° 34′ W	714	14.5	101.2	0.9
	59° 32′ N, 157° 5′ W	59° 25′ N, 157° 19′ W	696	9.8	66.9	0.6
	59° 48′ N, 156° 48′ W	59° 37′ N, 15° 76′ W	296	33.0	95.9	0.8
					TOTAL:	3.4
Susitna	Sunshine	Cook Inlet	862	77.7	657.0	5.8
	62° 17′ N, 150° 8′ W	Sunshine	555	16.8	91.2	0.8
	62° 24, 150° 10′ W	62° 17, 150° 8′ W	343	13.1	44.1	0.4
					TOTAL:	6.9

Table C-1 (continued)
Theoretical in-stream hydrokinetic power in segments of the major Alaska rivers in which the annual average flow rate exceeds 10,000 cfs (283 m³/s).

River	Segment start	Segment end	Q_{ave} (m³/s)	ΔH (m)	Power (MW)	Power (TWh/yr)
Porcupine	67° 25' N, 141° 1' N	66° 35' N, 145° 21' N	454	83.2	370.4	3.2
					TOTAL:	3.2
Colville	69° 54' N, 151° 29' W	Coast	319	14.9	46.7	0.4
	Umiat	69° 54' N, 151° 29' W	295	69.5	200.9	1.8
	65° 9' N, 154° 24' W	Umiat	218	105.5	225.0	2.0
					TOTAL:	4.1
Noatak	67° 8' N, 162° 36' W	Coast	312	4.0	12.2	0.1
	67° 17' N, 162° 40' W	67° 8' N, 162° 36' W	306	0.8	2.3	0.0
					TOTAL:	0.1
Copper	60° 43' N, 144° 39' W	Coast	1666	38.1	622.3	5.5
	60° 49' N, 144° 31' W	60° 43' N, 144° 39' W	1574	14.9	230.5	2.0
	61° 1' N, 144° 48' W	60° 49' N, 144° 31' W	1462	20.1	288.4	2.5
	61° 15' N, 144° 53' W	61° 1' N, 144° 48' W	1380	11.0	148.4	1.3
	61° 25' N, 144° 39' W	61° 15' N, 144° 53' W	1313	22.9	294.3	2.6
	61° 28'N, 144° 26' W	61° 25' N, 144° 39' W	1306	29.9	382.5	3.4
	61° 31' N, 144° 21' W	61° 28'N, 144° 26' W	822	9.5	76.1	0.7
	61° 31' N, 144° 18' W	61° 31' N, 144° 21' W	818	5.8	46.4	0.4
	61° 27' N, 144° 9' W	61° 31' N, 144° 18' W	806	15.9	125.3	1.1
	61° 23' N, 144° 5' W	61° 27' N, 144° 9' W	798	14.9	116.8	1.0
	61° 20' N, 143° 25' W	61° 23' N, 144° 5' W	778	61.0	464.8	4.1
	61° 11' N, 142° 48' W	61° 20' N, 143° 25' W	707	84.1	583.1	5.1

Table C-1 (continued)
Theoretical in-stream hydrokinetic power in segments of the major Alaska rivers in which the annual average flow rate exceeds 10,000 cfs (283 m³/s).

River	Segment start	Segment end	Q_{ave} (m³/s)	ΔH (m)	Power (MW)	Power (TWh/yr)
Copper	61° 4′ N, 142° 50′ W	61° 11′ N, 142° 52′ W	303	37.8	112.3	1.0
	61° 0′ N, 142° 43′ W	61° 4′ N, 142° 50′ W	302	32.3	95.6	0.8
	60° 57′ N, 142° 40′ W	61° 0′ N, 142° 43′ W	300	12.8	37.7	0.3
	61° 38′ N, 144° 35′ W	61° 30′ N, 144° 24′ W	521	22.0	112.2	1.0
	61° 41′ N, 144° 40′ W	61° 38′ N, 144° 35′ W	490	22.9	109.9	1.0
	61° 44′ N, 144° 48′ W	61° 41′ N, 144° 40′ W	465	16.2	73.7	0.6
	61° 50′ N, 145° 10′ W	61° 44′ N, 144° 48′ W	453	60.7	269.1	2.4
	61° 56′ N, 145° 20′ W	61° 50′ N, 145° 10′ W	446	23.2	101.4	0.9
	62° 3′ N, 145° 21′ W	61° 56′ N, 145° 20′ W	421	34.1	140.8	1.2
	62° 8′ N, 145° 26′ W	62° 3′ N, 145° 21′ W	344	24.7	83.3	0.7
					TOTAL:	39.6

The technically recoverable hydrokinetic resource for the selected Alaska river segments with average discharge greater than 10,000 cfs is presented in Table C-2.

Table C-2
Technically recoverable hydrokinetic resource (TWh/yr) in portions of selected Alaska rivers with average discharge greater than 10,000 cfs.

River	Technically Recoverable Resource (TWh/yr)
Yukon	13.2
Koyukuk	0.2
Tanana	0.7
Kuskokwim	1.1
Stikine	0.4
Kvichak	0.1
Nushagak	0.2
Susitna	0.5
Porcupine	0.1
Colville	0.1
Noatak	0.003
Copper	3.3
Total	19.9

In $Q493 the theoretical resource in Alaska was estimated to 59 TWh/yr in rivers with annual flow rates between 10,000 and 1,000 cfs. Examination of the dependence of recovery factor on discharge (Eq. 4.4) indicates that there would only be a positive recovery factor for flows greater than 7,000 cfs. In order to obtain an upper bound on an estimate of the technically recoverable resource in Alaska for flows between 10,000 and 1,000 cfs, we calculated the recovery factor (RF) based on a flow rate of 8,500 cfs (mid-point between 7,000 and 10,000 cfs), finding RF = 0.011. The Alaska technically recoverable resource for flows between 10,000 and 1,000 cfs was then estimated to be 0.6 TWh/yr for these low flow rivers. This brought the total technically recoverable in-stream hydrokinetic power in Alaska to 20.5 TWh/yr.

Appendix D: References

Atwater, J. and G. Lawrence. 2010. Power potential of a split channel. *REnewable Energy* **35**: 329-332.

Benson, M. A. and R. W. Carter. 1973. *A National Study of the Streamflow Data-Collection Program*. U.S. Geological Survey. Water-Supply Paper 2028.

Blanchfield, J., C. Garrett, P. Wild and A. Rowe. 2008. The extractable power from a channel linking a bay to the open ocean. *Proceedings of the Institution of Mechanical Engineers, Part A: Journal of Power and Energy* **222**(3): 289-297.

Bryden, I. and S. J. Couch. 2006. ME1 -- marine energy extraction: tidal resource analysis. *Renewable Energy* **31**(2): 133-139.

Couch, S. J. and I. G. Bryden. 2004. The impact of energy extraction on tidal flow development. *3rd IMarEST International Conference on Marine Renewable Energy 2004*.

Defne, Z., K. A. Haas and H. M. Fritz. 2011. GIS based multi-criteria assessment of tidal stream power potential: A case study for Georgia, USA. *Renewable and Sustainable Energy Reviews* **15**(5): 2310-2321.

EPRI (Electric Power Research Institute). 2006. *Methodology for Estimating Tidal Current Energy Resources and Power Production by Tidal In-Stream Energy Conversion (TISEC) Devices*. Palo Alto, CA. EPRI-TP-001-NA (Revision 3). September 29, 2006.

EPRI (Electric Power Research Institute). 2008. *System Level Design, Performance, Cost and Economic Assessment -- Alaska River In-Stream Power Plants*. Palo Alto, CA. EPRI-RP-006-Alaska. October 31, 2008.

Garrett, C. and P. Cummins. 2005. The power potential of tidal currents in channels. *Proceedings of the Royal Society. A.* **461**: 2563-2572.

Garrett, C. and P. Cummins. 2007. The efficiency of a turbine in a tidal channel. *Journal of Fluid Mechanics* **588**: 243-251.

Garrett, C. and P. Cummins. 2008. Limits to tidal current power. *Renewable Energy* **33**(11): 2485-2490.

Karsten, R. H., J. M. McMillan, M. J. Lickley and R. D. Haynes. 2008. Assessment of tidal current energy in the Minas Passage, Bay of Fundy. *Proceedings of the Institution of Mechanical Engineers, Part A: Journal of Power and Energy* **222**(5): 493-507.

Kartezhnikova, M. and T. M. Ravens. in review. Hydraulic impacts of hydrokinetic devices. *Journal of Hydraulic Engineering*.

Lunden, L. S. and A. S. Bahaj. 2007. Tidal energy resource assessment for tidal stream generators. *Journal of Power and Energy* **221**(2): 137-146.

McKay, L., T. R. Bondelid, A. Rea, C. Johnston, R. Moore and T. Dewald. 2012. *NHDPlus Verson 2: User Guide*. Prepared for U.S. Environmental Protection Agency, Office of Water. August 10, 2012.

Miller, G., J. Franceschi, W. Lese and J. Rico. 1986. *The Allocation of Kinetic Hydro Energy Conversion SYSTEMS(KHECS) in USA Drainage Basins: Regional Resource and Potential Power*. NYUDAS 86-151. August 1986.

Munson, B. R., D. F. Young and T. H. Okiishi. 2002. *Fundamentals of fluid mechanics*. Wiley, New York.

NRC-CHC (National Research Council of Canada - Canadian Hydraulic Centre). 2010. *Assessment of Canada's Hydrokinetic Power Potential: Phase I Report. Methodology and Data Review.*

Ortgega-Achury, S. L., W. H. McAnally, T. E. Davis and J. L. Martin. 2010. *Hydrokinetic Power Review*. Prepared for U.S. Army Corps of Engineers Research and Development Center, Vicksburg, Mississippi.

Polagye, B., P. C. Malte, M. Kawase and D. Durran. 2008. Effect of large-scale kinetic power extraction on time-dependent estuaries. *Journal of Power and Energy* **222**(5): 471-484.

Polagye, B. 2009. *Hydrodynamic Effects of Kinetic Power Extraction by In-Stream Tidal Turbines*. Doctoral dissertation. University of Washington, Seattle, WA.

Ravens, T. M., M. Johnson and M. Kartezhnikova. in preparation. Comparison of methods for estimating hydraulic impacts of hydrokinetic devices.

Shapiro, G. 2010. Effect of tidal stream power generation on the region-wide circulation in a shallow sea. *Ocean Science Discussions* **7**: 1785-1810.

Sun, X., J. P. Chick and I. Bryden. 2008. Laboratory-Scale Simulation of Energy Extraction from Tidal Currents. *Renewable Energy* **33**(6): 1267-1274.

Sutherland, G., M. Foreman and C. Garrett. 2007. Tidal current energy assessment for Johnstone Strait, Vancouver Island. *Journal of Power and Energy* **221** (2).

Walkington, I. and R. Burrows. 2009. Modelling tidal stream power potential. *Applied Ocean Research* **31**: 239-245.

Yang, Z. and T. Wang. 2011. *Assessment of Energy Removal Impacts on Physical Systems: Development of MHK Module and Analysis of Effects on Hydrodynamics.* U.S. Department of Energy, Pacific Northwest National Laboratory. September 2011.

The Electric Power Research Institute, Inc. (EPRI, www.epri.com) conducts research and development relating to the generation, delivery and use of electricity for the benefit of the public. An independent, nonprofit organization, EPRI brings together its scientists and engineers as well as experts from academia and industry to help address challenges in electricity, including reliability, efficiency, health, safety and the environment. EPRI also provides technology, policy and economic analyses to drive long-range research and development planning, and supports research in emerging technologies. EPRI's members represent approximately 90 percent of the electricity generated and delivered in the United States, and international participation extends to more than 30 countries. EPRI's principal offices and laboratories are located in Palo Alto, Calif.; Charlotte, N.C.; Knoxville, Tenn.; and Lenox, Mass.

Together...Shaping the Future of Electricity

Program:

Environment

1026880